



# 1                    **Characterization of offline analysis of particulate matter with** 2                    **FIGAERO-CIMS**

3                    Jing Cai<sup>1,2,#</sup>, Kaspar R. Daellenbach<sup>1,2,3,#,\*</sup>, Cheng Wu<sup>4,5</sup>, Yan Zheng<sup>6</sup>, Feixue Zheng<sup>1</sup>, Wei Du<sup>1,2</sup>, Sophie L. Haslett<sup>4</sup>,  
4                    Qi Chen<sup>6</sup>, Markku Kulmala<sup>1,2</sup>, Claudia Mohr<sup>4,\*</sup>

5                    <sup>1</sup> Aerosol and Haze Laboratory, Beijing Advanced Innovation Center for Soft Matter Science and Engineering,  
6                    Beijing University of Chemical Technology, Beijing 100029, China

7                    <sup>2</sup> Institute for Atmospheric and Earth System Research, Faculty of Science, University of Helsinki, Helsinki 00014,  
8                    Finland

9                    <sup>3</sup> Laboratory of Atmospheric Chemistry, Paul Scherrer Institute, Villigen, Switzerland.

10                    <sup>4</sup> Department of Environmental Science, Stockholm University, Stockholm, 11418, Sweden

11                    <sup>5</sup> Department of Chemistry and Molecular Biology, Atmospheric Science, University of Gothenburg, Gothenburg,  
12                    SE-412 96, Sweden

13                    <sup>6</sup> State Key Joint Laboratory of Environmental Simulation and Pollution Control, Beijing Innovation Center for  
14                    Engineering Science and Advanced Technology, College of Environmental Science and Engineering, Peking  
15                    University, Beijing, 100871, China

16                    # These authors contributed equally to this work.

17                    Correspondence to: [kaspar.dallenbach@helsinki.fi](mailto:kaspar.dallenbach@helsinki.fi) and [claudia.mohr@aces.su.se](mailto:claudia.mohr@aces.su.se)

18                    **Abstract:** Measurements of the molecular composition of organic aerosol (OA) constituents improve our  
19                    understanding of sources, formation processes, and physicochemical properties of OA. One instrument providing  
20                    such data at a time resolution of minutes to hours is the Chemical Ionization time-of-flight Mass Spectrometer  
21                    with Filter Inlet for Gases and AEROSols (FIGAERO-CIMS). The technique collects particles on a filter, which  
22                    are subsequently desorbed, and the evaporated molecules are ionized and analyzed in the mass spectrometer.  
23                    However, long-term measurements using this technique and/or field deployments at several sites simultaneously,  
24                    require substantial human and financial resources. The analysis of filter samples collected outside the instrument  
25                    (offline) may provide a more cost-efficient alternative and makes this technology available for the large number  
26                    of particle filter samples collected routinely at many different sites globally. Filter-based offline use of the  
27                    FIGAERO-CIMS limits this method albeit to particle-phase analyses, likely at reduced time resolution compared  
28                    to online deployments. Here we present the application and assessment of offline FIGAERO-CIMS, using Teflon  
29                    and Quartz fiber filter samples that were collected in autumn 2018 in urban Beijing. We demonstrate the feasibility  
30                    of the offline application with “sandwich” sample preparation for the identified over 900 organic compounds with  
31                    (1) high signal-to-noise ratios, (2) high repeatability, and (3) linear signal response to the filter loadings.  
32                    Comparable overall signals were observed between the Quartz fiber and Teflon filters for 12-h and 24-h samples,  
33                    but with larger signals for semi-volatile compounds for the Quartz fiber filters, likely due to adsorption artifacts.  
34                    We also compare desorption profile (thermogram) shapes for the two filter materials. Thermograms are used to  
35                    derive volatility qualitatively based on the desorption temperature at which the maximum signal intensity of a  
36                    compound is observed ( $T_{\max}$ ). While we find that  $T_{\max}$  can be determined with high repeatability for one filter type,  
37                    we observe considerable differences in  $T_{\max}$  between the Quartz and Teflon filters, warranting further investigation  
38                    into the thermal desorption characteristics of different filter types. Overall, this study provides a basis for  
39                    expanding OA molecular characterization by FIGAERO-CIMS to situations where and when deployment of the  
40                    instrument itself is not possible.

## 41                    **1. Introduction**



42 Molecular information on organic aerosol (OA) composition is important for understanding the role that OA  
43 plays in the atmosphere regarding its impacts on air quality, human health, and the climate (Daellenbach et al.,  
44 2020; Huang et al., 2014; Cappa et al., 2012; Yao et al., 2018; Riipinen et al., 2012). Such data can be obtained  
45 from offline filter collection and analysis in the laboratory using optical (e.g. Fourier transform infrared  
46 spectroscopy, FTIR) and magnetic (e.g. Nuclear magnetic resonance spectroscopy, NMR) spectroscopy or, more  
47 commonly, high-resolution mass spectrometer methods, which include gas/liquid chromatography coupled to  
48 mass spectrometry (GC/LC-MS), ultrahigh-performance liquid chromatography coupled to Orbitrap mass  
49 spectrometry and electrospray ionization mass spectrometry (ESI-MS) (Noziere et al., 2015). In contrast, online  
50 mass spectrometers provide direct and in-situ information on particles' molecular composition, e.g. the filter inlet  
51 for gases and aerosols coupled to a high-resolution time-of-flight chemical ionization mass spectrometer  
52 (FIGAERO-HR-ToF-CIMS, Aerodyne Research Inc., US, hereafter FIGAERO-CIMS (Lopez-Hilfiker et al.,  
53 2014)) or the extractive electrospray ionization time-of-flight mass spectrometer (EESI-MS) (Lopez-Hilfiker et  
54 al., 2019). Since the particle-phase measurement by FIGAERO-CIMS is filter-based, it has the potential to be used  
55 for offline analysis. Briefly, in the FIGAERO, particles are collected on a Teflon<sup>®</sup> (hereafter Teflon) filter and  
56 analyzed via thermal desorption. When coupled to a high-resolution time-of-flight chemical-ionization mass  
57 spectrometer (hereafter CIMS), molecular composition information of inorganic and organic aerosol compounds  
58 that evaporate at temperatures up to 200 °C can be achieved. Having the advantage of combining molecular  
59 composition and volatility information, the FIGAERO-CIMS has been widely used for measuring OA compounds  
60 in many different environments including e.g. forests (Lopez-Hilfiker et al., 2016; Lee et al., 2016; Lee et al., 2018;  
61 Mohr et al., 2019), rural and urban areas (Le Breton et al., 2019; Huang et al., 2019b; Cai et al., 2022), and indoor  
62 air (Farmer et al., 2019).

63 Both online and offline techniques have their advantages and disadvantages and are associated with artefacts  
64 (Turpin and Lim, 2001; Turpin et al., 2000). Online instruments generally allow for measurements at higher time  
65 resolution, which is an advantage when studying rapid atmospheric processes, and no sample storage is needed  
66 before analysis. However, the deployment of the FIGAERO-CIMS outside the laboratory requires a well-equipped  
67 site that is easily accessible. In addition, long-term maintenance of these complex mass spectrometers needs  
68 substantial human and financial resources. Therefore, deployments are often achieved only for short periods (i.e.  
69 campaigns lasting from a couple of weeks to months), which limits the application of this technique for monitoring  
70 and simultaneous measurements at multiple sites. Furthermore, FIGAERO gas-phase measurements have to be  
71 interrupted regularly for particle-phase analysis in online usage, which could be a problem for measurements  
72 requiring high time resolution data (e.g. chamber studies). Using the FIGAERO-CIMS for analyzing filters  
73 collected elsewhere ("offline application") may therefore provide a valid alternative for long-term monitoring or  
74 simultaneous measurements at multiple sites. Whereas the online FIGAERO-CIMS technique typically uses  
75 Teflon filters to reduce interferences from the gas phase, Quartz fiber filters are widely used for offline sampling  
76 of OA due to their high melting point and insolubility in water and typical organic solvents (Watson and Chow,  
77 2002; Tao et al., 2017; Schauer et al., 2002; Gustafson and Dickhut, 1997). Up to now, only a few studies have  
78 used the FIGAERO-CIMS in offline mode with Teflon filters (Siegel et al., 2020; Huang et al., 2019a), and an in-  
79 depth characterization of the method is missing. The performance of Quartz fiber filters in FIGAERO-CIMS needs  
80 to be assessed and compared to Teflon filters.

81 Here, we describe the application of FIGAERO-CIMS in offline mode for the analysis of particles deposited on  
82 Teflon and Quartz fiber filters in urban Beijing during the autumn and winter of 2018. The filter deposition time  
83 varies from 30 min to 24 h. We assess the performance of FIGAERO-CIMS for offline characterization of OA as  
84 well as inorganic compounds and discuss background determination, reproducibility, and linearity of response for  
85 the two filter types. We describe filter handling and offline analysis procedures and show the comparison of signals  
86 from different mass loadings collected on both filter types. The utility of the FIGAERO for offline use is  
87 demonstrated in this study. The potential to broaden its application for OA component measurements in future  
88 research is also discussed.

## 89 2. Methods



## 90 2.1 Filter sampling

91 The sampling site is situated on the west campus of the Beijing University of Chemical Technology (BUCT, 39°  
92 56'31" N, 116°17'50" E). BUCT is located near the West Third Ring Road of Beijing, surrounded by residential  
93 areas. A more detailed description of the sampling site can be found elsewhere (Cai et al., 2020; Kontkanen et al.,  
94 2020; Liu et al., 2020; Yao et al., 2020; Fan et al., 2021; Guo et al., 2021). From November to December 2018,  
95 samples of fine particulate matter with an aerodynamic diameter of up to 2.5  $\mu\text{m}$  ( $\text{PM}_{2.5}$ ) were collected by a four-  
96 channel sampler (TH-16A, Tianhong Co., China) with a sampling flow rate of 16.7  $\text{L min}^{-1}$ , installed on the rooftop  
97 of a five-floor building (~20m above ground). Both Teflon (Zefluor® PTFE membrane, 1  $\mu\text{m}$  pore size, 47 mm  
98 diameter, Pall Corp., US) and Quartz fiber filters (7202, 47 mm diameter, Pall Corp., US) were collected  
99 simultaneously at separate channels equipped with separate  $\text{PM}_{2.5}$  cyclones of the sampler.

100 To investigate the influence of filter mass loadings and collection time on the signal response, the following filter  
101 samples were taken: (1) 5 pairs of samples (Teflon/Quartz fiber filters) with 30 min deposition time on Dec 15,  
102 2018 between 14:00 to 16:30 (Table 1). At the same time, an additional pair of Teflon/Quartz samples were  
103 deposited for 2.5 hours using the other two separate channels of the sampler. (2) 12-h samples of Quartz/Teflon  
104 filters from Oct 26 to Oct 30 and Nov 3 to Nov 24 (here only the Quartz filters from Nov 3 to Nov 16 were analyzed  
105 (in total 27 pair of samples), shown in Table 1). (3) 24-h Quartz/Teflon samples from Oct 26 to Oct 30 and Nov 3  
106 to Nov 25 (here only one pair of Teflon/Quartz filters was analyzed, shown in Table 1). During the last sampling  
107 period, high  $\text{PM}_{2.5}$  and relative humidity (RH) conditions prevailed (Nov 3: 181  $\mu\text{g m}^{-3}$ , 60%, and Nov 13: 227  $\mu\text{g}$   
108  $\text{m}^{-3}$ , 75%), and the channel of the 24-h sampling Teflon filter got clogged. Thus, only one pair of 24-h  
109 Teflon/Quartz samples from this period was analyzed (Table 1).

110 Detailed information on the sampling protocol is listed in Table 1. Three pairs (Teflon/Quartz) of field blank  
111 samples were also collected during the sampling period. Before sampling, Teflon filters were baked for 2 hours at  
112 200 °C, which is much longer than the typical desorption time for FIGAERO-CIMS online usage (Ylisirniö et al.,  
113 2021), and Quartz filters for 4.5 hours at 550 °C (Liu et al., 2016) in order to minimize contamination. After  
114 sampling, samples were put in filter holders wrapped in pre-baked aluminum foils, individually sealed in a sealed  
115 bag and stored in a freezer at -20 °C for 7 months until being analyzed in the laboratory.

116 To calculate the OA mass loadings of the samples, an online Time-of-Flight-Aerosol Chemical Speciation  
117 Monitor (Aerodyne Research Inc., US, hereafter ToF-ACSM) equipped with a  $\text{PM}_{2.5}$  lens and standard vaporizer  
118 was operated during the sampling period at the same site. Details of the ToF-ACSM settings can be found in Cai  
119 et al. (2022).

120

121 Table 1: Testing objectives, filter deposition dates and times, flows, filter material (T = Teflon, Q = Quartz fiber),  
122 filter mass loadings of OA, number of samples, and number of sample repeats (filter punches) for the same filter.

123



124

Testing objective	Sampling date	Sampling time	Filter material	OA loading [ $\mu\text{g}$ ] per punch (punch diameter, area)	Number of samples/repeats
(1) Baseline subtraction tests, (2) reproducibility tests, (3) filter type comparison	Dec 15 14:00 – 16:30 (30 min-interval)	30 min	T & Q	$1.7 \times 10^{-2}$ – $2.0 \times 10^{-2}$ (2 mm, 0.031 cm <sup>2</sup> )	1/1
	Dec 15 14:00 – 16:30	2.5 h	T & Q	$9.1 \times 10^{-2}$ (2 mm, 0.031 cm <sup>2</sup> )	1/3 for repeats
(1) Reheating tests, (2) filter type comparison	Nov 8 21:30– Nov 9 9:00	12 h	T & Q	$6.5 \times 10^{-1}$ (2 mm, 0.031 cm <sup>2</sup> )	1/1
Reheating tests	Nov 12 21:30– Nov 13 9:00	12 h	Q	0.75 (2 mm, 0.031 cm <sup>2</sup> )	1/1
Reheating tests	Nov 13 21:30– Nov 14 9:00	12 h	Q	1.2 (2 mm, 0.031 cm <sup>2</sup> )	1/1
(1) Filter type comparison, (2) different ramping protocols for 2 mm punch, (3) linearity response for signals from different filter punch areas	Nov 24 9:30– 9:00 25	24 h	T & Q	1.2 (2 mm, 0.031 cm <sup>2</sup> )	1/3 for repeats and 1/3 for different ramping protocols
				2.7 (3 mm, 0.071 cm <sup>2</sup> )	1/1
				4.8 (4 mm, 0.13 cm <sup>2</sup> )	1/1
				15 (7 mm, 0.38 cm <sup>2</sup> )	1/1
Comparison of 12-h signals to ToF-ACSM	Nov 3 to Nov 16	12 h	Q	$5.0 \times 10^{-2}$ – 1.2 (2 mm, 0.031 cm <sup>2</sup> )	27/1



125

## 126 **2.2 Offline application of FIGAERO-CIMS**

### 127 **2.2.1 Measurement approach**

#### 128 **2.2.1.1 FIGAERO-CIMS setup**

129 The molecular composition of OA collected on the filter samples was characterized with FIGAERO-CIMS using  
130 iodide (I<sup>-</sup>) as the reagent ion. In typical online FIGAERO-CIMS operation, particles are collected on a filter  
131 (Zefluor<sup>®</sup> Teflon filters) with a sampling time of a few minutes to hours and then thermally desorbed by a flow of  
132 temperature-controlled ultra-pure nitrogen (99.999 %) immediately following deposition. The thermally desorbed  
133 compounds are charged by clustering with I<sup>-</sup>, which is typically generated through the exposure of methyl iodide  
134 to an X-ray or radioactive source for FIGAERO-CIMS (Po<sup>210</sup> in our study). In this study, we used the FIGAERO-  
135 CIMS in the laboratory to analyze filter samples collected earlier in the field. These samples were placed manually  
136 one by one in the dedicated filter holder of the FIGAERO-CIMS and the desorption procedure was started (see  
137 2.2.1.3).

#### 138 **2.2.1.2 Sample preparation and test design**

139 Since the total particle mass collected on one filter was generally too large to be analyzed at once in its entirety  
140 by FIGAERO-CIMS (due to the risk of titration of the reagent ion), we only analyzed small circular punches of  
141 the collected filters. The default punching area was  $3.1 \times 10^{-2} \text{ cm}^2$  (punch diameter  $d=2 \text{ mm}$ ). In addition, to test the  
142 linearity of response to sample mass loadings, punch areas for the same filter were varied between  $3.1 \times 10^{-2} \text{ cm}^2$   
143 ( $d=2 \text{ mm}$ ) and  $0.38 \text{ cm}^2$  ( $d=7 \text{ mm}$ ), resulting in variation in mass loadings by a factor of 10 (shown in Table 1).  
144 Since the filter punches were too small for the filter holder of the FIGAERO, we put them between two pre-baked  
145 originally sized ( $d=25 \text{ mm}$ ) Zefluor<sup>®</sup> Teflon filters (“sandwich technique”, Fig. 1a). Field blanks were prepared  
146 analogously.

147 The OA mass loadings of the filter punches were estimated with the co-located ToF-ACSM in this study (details  
148 shown in Table 1). To test the performance of the method, we did the following tests (Fig. 1, Table 1): (1) reheating  
149 a few filters to determine backgrounds (see section 2.2.4), (2) assess different background subtraction methods,  
150 (3) reproducibility of signals from the same filter (section 3.4), (3) the linearity of signal response from different  
151 punching areas from the same filter (section 3.4), (3) comparing signals from different ramping protocols (section  
152 2.2.1.3), (4) comparison between and offline FIGAERO-CIMS and online ToF-ACSM (section 3.5), (5) signals  
153 from different filter types (section 3.6), and (6) thermograms from different types of filters (section 3.7).

#### 154 **2.2.1.3 Temperature ramping protocols**

155 Reagent ion depletion is undesired as it can create non-linearities in the instrument response (Koss et al., 2018;  
156 Zheng et al., 2021). To avoid reagent ion depletion in FIGAERO-CIMS, the concentration of sample ions entering  
157 the instrument is controlled, typically by modifying the particle mass loading on the filter and/or the heating rate.  
158 While the particle mass loading can be varied easily when operating the FIGAERO-CIMS online through  
159 adjustment of sampling time and flow, in offline mode with pre-collected samples this can only be modified by  
160 the fraction of filter surface analyzed. For our Beijing filter samples, even when using the smallest punch sizes  
161 ( $3.1 \times 10^{-2} \text{ cm}^2$ ), mass loadings of especially nitric acid (HNO<sub>3</sub>) were still high enough to lead to titration of the  
162 reagent ion. We note that this can also be an issue for online measurements in presence of high nitrate  
163 concentrations, e.g. in highly polluted areas. In order to reduce reagent ion depletion between 60 °C to 105 °C  
164 desorption temperature, where HNO<sub>3</sub> exhibits a maximum signal, we used a heating protocol with a non-uniform  
165 temperature ramping procedure. Instead of ramping from room temperature to 200 °C with a constant heating rate,  
166 we divided the temperature ramp into several periods: (1) from room temperature (~25 °C) to 60 °C in 8 min

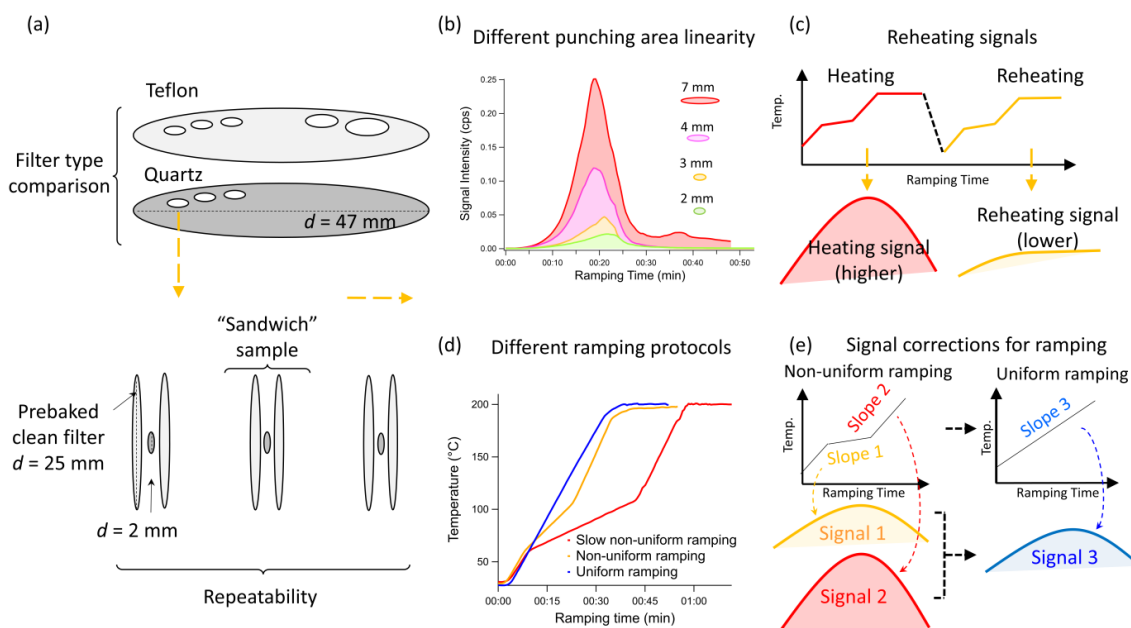


167 (4.4 °C min<sup>-1</sup>), (2) from 60 °C to 105 °C in 15 min (3 °C min<sup>-1</sup>), (3) from 105 °C to 200 °C in 12 min (7.9 °C min<sup>-1</sup>).  
168 The ramp period was followed by a 20-minute soaking period (200 °C) to allow signals to go to background  
169 levels. We called this temperature ramping protocol non-uniform temperature ramping and used it as the default  
170 desorption procedure in this study. The maximum reagent ion depletion achieved in this way was ~35% for the  
171 samples with the highest mass loadings on a 2 mm punch, which was mostly used in this study. We also tested  
172 two alternative heating protocols:

- 173 1) Slow non-uniform temperature ramping: Same as the non-uniform ramping protocol, but with (2)  
174 slowed down to 1.5 °C min<sup>-1</sup>. The total heating time for this protocol was 70 minutes, and the  
175 maximum reagent ion depletion was ~20%.
- 176 2) Uniform temperature ramping: The temperature was increased from room temperature to 200 °C  
177 in 31.5 min (5.7 °C min<sup>-1</sup>). Including the 20 min soak, the total heating was 51.5 minutes, and the  
178 maximum reagent ion depletion was around 50%. In order to limit reagent ion depletion, the  
179 heating rate was 1.8–3.5 times slower than typical rates used for online FIGAERO-CIMS  
180 applications (10–20 °C min<sup>-1</sup> (Thornton et al., 2020)).

181 The 3 temperature ramping protocols are displayed in Fig. 1d. As different heating rates lead to different  
182 thermogram shapes and T<sub>max</sub> for individual compounds, we developed a correction method in an effort to be able  
183 to compare desorption-derived volatility for the different ramping protocols. This will be further discussed in  
184 section 3.3.

185



186

187 **Figure 1.** Schematic of the tests conducted in this study, (a) sample preparation using punching areas of different the  
188 Teflon and Quartz fiber filters and squeezing them between two original-sized filters for analysis, (b) signal intensities of  
189 different punching areas from the same sample with the same analytical procedure, (c) reheating tests by conducting two  
190 consecutive heating cycles, (d) different temperature procedures, and (e) signal intensity correction from non-uniform  
191 ramping to uniform ramping.

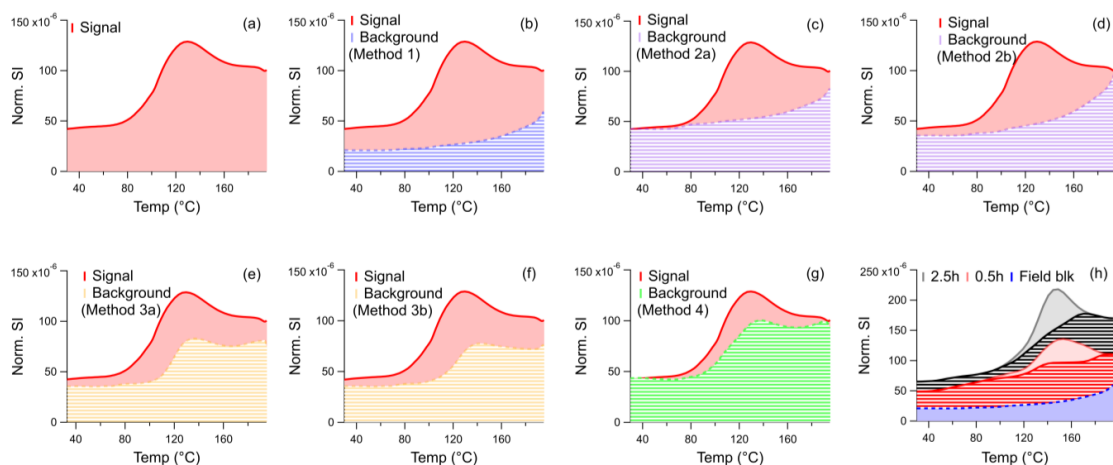


## 192 2.2.2 Data analysis

193 In this study, FIGAERO-CIMS data were analyzed with the Tofware package (v.3.1.0, Tofwerk, Switzerland,  
194 and Aerodyne, US) within the Igor Pro software (v.7.08, Wavemetrics, US). Mass accuracies of low- to high-mass  
195 species (~130 to 500 Da) were within  $\pm 10$  ppm for all the samples. A total of ~1,200 peaks were found in the range  
196 of 46 and 500 Da, of which 916 were identified as organic species. Detailed information about the identified  
197 chemical compounds can be found in Cai et al. (2022). The total signal of a compound per filter sample, defined  
198 as the integrated signals ( $I_s$ ), was calculated by integrating the entire thermogram (ramping and soaking,  
199 normalized by the signals of  $I$ ). Signals of the first 1.5 min of ramping and the last 1.5 min of soaking periods  
200 were excluded in order to remove potential interference from switching to and from the heating status. In this study,  
201 we use the term CHOX to represent all organic compounds identified by FIGAERO-CIMS,  $C_{x \geq 1}H_{y \geq 1}O_{z \geq 1}X_{0-n}$ ,  
202 detected as clustered with  $I^-$ , with X being different atoms including N, S, Cl, or a combination of them.

## 203 2.2.3 Background subtraction

204 The background in offline FIGAERO-CIMS is a combination of instrument background and field blank. The  
205 field blanks provide information on sampling and handling artefacts, while the instrument background is mainly  
206 from (1) the desorption of semi-volatile or low-volatile compounds adsorbed on instrument surfaces (such as the  
207 ion-molecular reaction region (IMR)), and (2) impurity of the reagent ion precursors and carrier gases. Thus,  
208 instrument background signal can vary for different samples and depending on instrument status. For FIGAERO-  
209 CIMS online deployments, frequent blank measurements and calibrations are recommended (Bannan et al., 2018;  
210 Thornton et al., 2020). The common method for online FIGAERO-CIMS of placing an additional filter upstream  
211 of the FIGAERO filter is impossible for offline pre-sampled filters. Given  $I$  the large variation of the filter sample  
212 loadings ( $\sim 1 \times 10^{-2} \mu\text{g} - 1.2 \mu\text{g}$ ), which influences the number of compounds that can potentially adsorb to  
213 instrument surfaces, 2) the general scarcity of field blanks in offline mode compared to background filter samples  
214 in online FIGAERO-CIMS, and 3) that the instrument background can be influenced by instrument history very  
215 different from the offline sample due to the temporal separation of sample and analysis, choosing an appropriate  
216 instrumental and field blank determination method is crucial and challenging for offline FIGAERO-CIMS analysis.  
217 Here we describe and discuss performance of 6 different background subtraction methods (schematically shown  
218 in Fig. 2):



219

220 **Figure 2.** Schematic of a compound's signal and background thermograms for different background determination methods.  
221 The x-axis is the temperature during ramping, and the y-axis is the signal intensity normalized by the primary ion ( $I^-$ ). (a) total  
222 sample signal of a model compound without blank subtraction, (b) Method 1: field blank only, (c) Method 2a: scaling field  
223 blank to the start of ramping, (d) Method 2b: scaling field blank to the end of soaking, (e) Method 3a: reheating of a subset of



224 filters, and using the average signal ratio from reheated and heated filters as background signal for all filters (individual  
225 compound-based), (f) Method 3b: reheating of a subset of filters, and using an exponential fit to the entire mass range of the  
226 average signal ratio from reheated and heated filters as background signal for all filters, (g) Method 4: thermal baseline using  
227 a spline algorithm, and (h) one 0.5-h and one 2.5-h sample with blank-subtraction. Ideally, the  $I_s$  of the 2.5-hour collection  
228 sample ( $I_{s_{2.5h}}$ ) would be close to the sum of the 5 paralleled 0.5-hour collection sample ( $I_{s_{0.5h}}$ ).

229 **Method 1:** Background is the average integrated signal intensity ( $I_s$ , the integrated signal of the thermograms  
230 shown in Fig. 2a) of field blanks ( $\overline{I_{s_{field\ blk,l}}}$ ), which are three in our case (Fig. 2b). The integrated background-  
231 subtracted signal for compound  $i$  ( $I_{s_{blksub,i}}$ ) is then  $I_{s_i} - \overline{I_{s_{field\ blk,l}}}$ .

232 **Method 2:** Background is field blank average ( $\overline{I_{s_{field\ blk,l}}}$ , see Method 1) scaled to the ratio of ambient sample  
233 and field blank signals during a reference period (ref period) – either prior to the start of heating (the first 1.5 to 3  
234 min of the ramping procedure before the temperature starts to increase, Method 2a or at the end of the soaking (the  
235 last 1.5 to 3 min of the soaking period, Method 2b). Method 2 corrects for variation in instrument background that  
236 is not necessarily related to the sample to be analyzed. The integrated background-subtracted signal for compound  
237  $i$  ( $I_{s_{blksub,i}}$ ) is then

$$238 \quad I_{s_{blksub,i}} = \int I_{sample,ij} - \int I_{field\ blk,ij} \times \frac{\int^{ref\ period} I_{s_{i,ambient}}}{\int^{ref\ period} I_{s_{i,field\ blk}}} \quad (1)$$

239 By using Method 2a, it is assumed that the signal measured before heating, but with the filter already in place, is  
240 due to instrument background, which can vary between the measurement of a sample filter and a blank filter (Fig.  
241 2c). However, this method may lead to underestimation of the sample signal for compounds that already evaporate  
242 at room temperature.

243 By using Method 2b, it is assumed that the signal measured at the end of soaking is due to instrument background,  
244 which can vary between the measurement of a sample filter and a blank filter. The variation in instrument  
245 background is taken into account at maximum heating temperature (200 °C) and thus elevated temperature of  
246 surfaces downstream of the filter, and at the end of the soaking period when presumably all material that can  
247 evaporate from the filter has evaporated (shown in Fig. S1).

248 **Method 3:** In this method (Siegel et al., 2021), the instrument background is assessed by heating the same filter  
249 twice, assuming that during the first heating cycle, all detectable material has evaporated, and that what is measured  
250 in a reheating cycle is the instrument background signal. Ideally, reheating would be done for each sample  
251 individually. Since this was not done for our dataset, the instrument background determined based on a few reheats  
252 (3 in our case, the details of the reheating samples are shown in Table 1) had to be extrapolated to all samples  
253 (Method 3a and 3b). It is clearly shown that the signals from the reheating cycle are much lower than those from  
254 the first heating (Fig. S1) without a clear peak in thermograms for both filter types, suggesting sampled compounds  
255 were well desorbed in the original heating cycle. Simple reheating does not consider the field blanks, which need  
256 to be subtracted in addition.

257 For Method 3a we assumed that the ratio of the integrated signal of the second heating cycle (heating C2) and first  
258 heating cycle (heating C1) of the same filter is influenced by volatility and therefore compound-dependent. Here  
259 we used the average ratio from 3 reheating tests done for this dataset (Fig. S2). The distribution of the ratios is  
260 shown in Fig. S3. The  $I_{s_{blksub,i}}$  was then calculated following Eq. 2, where the instrument background is the fraction  
261 of the sample signal established from the re-heating, and added to the signal from the field blank, which is  
262 calculated in the same way.

$$263 \quad I_{s_{blksub,i}} = \left( I_{s_{sample,i}} - I_{s_{sample,i}} \times I_{s_{i, \left( \begin{smallmatrix} heating\ C2,i \\ heating\ C1,i \end{smallmatrix} \right)}} \right) \\ 264 \quad - \left( I_{s_{field\ blk,i}} - I_{s_{field\ blk,i}} \times I_{s_{i, \left( \begin{smallmatrix} heating\ C2,i \\ heating\ C1,i \end{smallmatrix} \right)}} \right) \quad (2)$$





265 For Method 3b, we assumed that the ratio of heating C2 to heating C1 exhibits a signal dependency (relatively  
266 higher background for compounds with lower signal), calculated using an exponential fit to the data from the 3  
267 reheat tests (Fig. S4) using Eq. (3) with the constants A, B, and C. The field blanks are calculated in the same way.  
268 Then the  $I_{S_{blksub}}$  can be calculated as in Eq. (2)

$$269 \quad I_{S_{i, \left( \frac{\text{heating C2}, i}{\text{heating C1}, i} \right)}} = A + B \times \exp(I_{S_{sample}, i} + C) \quad (3)$$

270 **Method 4:** Thermal baseline subtraction. In this method, we determined for every thermogram of each compound  
271 a background thermogram termed thermal baseline ( $I_{S_{thbs}}$ ). The thermal baseline was computed using a spline  
272 algorithm initially developed by Wang et al. (2018) for determining the background concentration of a pollutant  
273 using its concentration time series (by determining the spline of background from varying time intervals).  
274 Thermogram data were pre-averaged to 1.8 mins (corresponding to 4 data points of the original time resolution of  
275 27s) to reduce noise for the thermal baseline computation. Field blanks were handled in the same way. Thus, the  
276 blank-subtracted signal  $I_{S_{blksub}}$  of a compound  $i$  is:

$$277 \quad I_{S_{blksub}, i} = I_{S_{sample, blksub}, i} - I_{S_{field\ blk, blksub}, i}$$
$$278 \quad = \left( \int I_{S_{sample}, i, j} - I_{S_{sample, thbs}, i} \right) - \left( \int I_{S_{field\ blk}, i, j} - I_{S_{field\ blk, thbs}, i} \right) \quad (4)$$

280  $I_{S_{sample, thbs}, i}$  and  $I_{S_{field\ blk, thbs}, i}$  represent the thermal baseline of compound  $i$  for samples and field blanks, respectively.

#### 281 2.2.4 Thermograms and $T_{max}$ recovery

282 The amount of compounds coming off the filter at a certain temperature varies as a function of temperature  
283 ramping rates, resulting in different thermogram shapes and  $T_{max}$  (shown in Fig. 1d). This is especially important  
284 in our case for the non-uniform ramping protocols. In an attempt to make the different cases comparable for  
285 qualitative volatility studies, we developed a thermogram correction where the blank-subtracted signal as a  
286 function of temperature for each compound  $i$  is re-distributed to constant temperature intervals (Eq. (5)):

$$287 \quad I_{thermocorrected, i, j} = \int_{T-\Delta t}^T I_{sample, blksub, i, j} dT \quad (5)$$

288 Considering the  $\sim 2$  °C variation in thermogram reproducibility reported from an online FIGAERO-CIMS study  
289 (Lopez-Hilfiker et al., 2014), the temperature interval  $\Delta T$  used in this study is 3°C.

290

### 291 3. Results

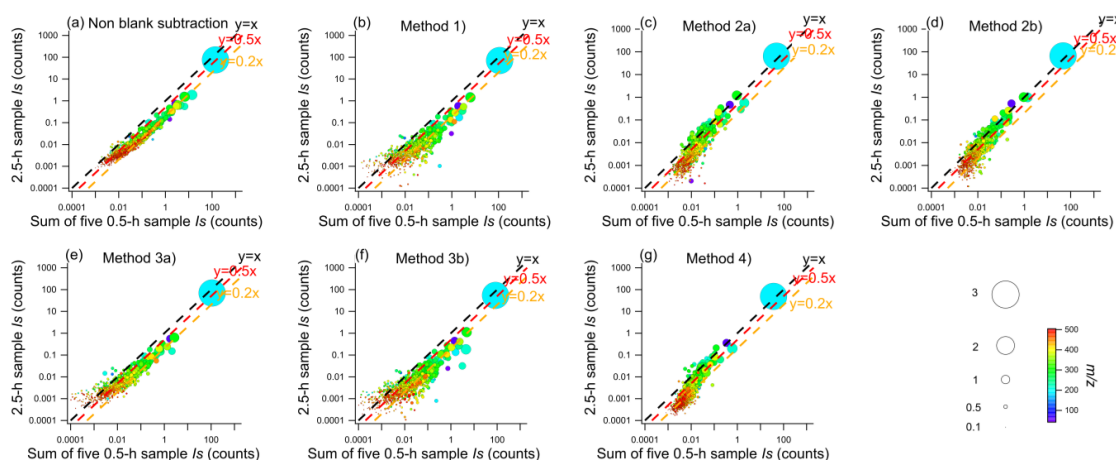
#### 292 3.1 Assessment of the background: Signal comparison between different blank subtraction methods

293 To assess the influence of the 6 background methods on the resulting signal, Quartz fiber filter samples from 5  
294 different 0.5-h samples (OA:  $\sim 2.0 \times 10^{-2}$   $\mu\text{g}$  for each punch) and a 2.5 h sample collected in parallel (OA:  $9.1 \times 10^{-2}$   
295  $\mu\text{g}$ ) were used, and the sum of their background-subtracted integrated signals ( $I_{S_{blksub}}$ ) compared (Fig.2 h). Without  
296 background subtraction, the sum of the signals from the five 0.5-h samples was generally higher than the  $I_S$  of the  
297 2.5-h sample (shown in Fig. 3a). An exception to this is  $\text{HNO}_3$ , which has the highest signal of all compounds and  
298 therefore is the least influenced by background. The higher  $I_S$  for the sum of the five 0.5-h samples is likely because  
299 of the low signal-to-noise ratio compared to the 2.5-h sample. Subtracting only the field blank (Method 1) therefore  
300 yielded the same result (Fig. 3b). Scaling the heating baseline (Method 2a and 2b) led to a better agreement between  
301 the sum of the five 0.5-h and the 2.5-h samples (Figs. 3c and d). Compounds with high abundance generally fall  
302 on a 1:1 line (slope range 0.5–2) by using these two background subtraction methods. With the thermal baseline  
303 subtraction method (Method 4), results were comparable between 2.5-h and five 0.5-h samples. For the approach



304 using filter reheating (Method 3), there was lesser agreement between the sum of the 0.5-h samples and the 2.5-h  
305 sample (Figs. 3e and 3f). We speculate that this could be improved with a reheating cycle for every sample.

306 In general, as expected, high mass loadings are less sensitive to the various background subtraction methods due  
307 to the higher signal-to-noise ratio (for example, 12-h/24-h sampling with OA loading of  $\sim 1 \mu\text{g}$ , Fig. S5). Besides  
308 filter loadings, baseline levels can also be influenced by the properties of compounds (e.g. stickiness) and  
309 instrument geometry. In summary, of all background subtraction methods shown here, Methods 2a, 2b, and 4  
310 achieved the best agreement in signal intensities between the sum of 0.5-h and 2.5-h samples (Fig. S6). With these  
311 methods, 82% to 93% of high-signal compounds (25% highest signal) fell into a signal ratio of  $\sim 1$  (0–2). This  
312 shows the importance of assessing the instrument background right, especially for compounds with low signal.



313

314 **Figure 3.** Comparison of the integrated signals ( $I_s$ ) for the 2.5-h versus sum of 0.5-h samples (a) without blank subtraction,  
315 with blank subtraction using (b) Method 1, (c) Method 2a, (d) Method 2b, (e) Method 3a, (f) Method 3b, (g) Method 4. The  
316 size of dots is proportional to the 4<sup>th</sup> root of integrated signal intensities of compounds, and they are color-coded by the ions'  
317  $m/z$  (mass-to-charge ratio).

318 In this study, we applied Method 2b in the following discussions due to its better performance for the compounds  
319 with both higher ( $I_s > 0.1$  counts) and lower signal ( $I_s < 0.01$  counts, Fig. 3d). First, we examined the signal-to-noise  
320 ratios for offline FIGAERO-CIMS, defined as the ratio of the blank-subtracted signal to the standard deviation  
321 (STDs) of the background determined using method 2b per compound. Most of the identified compounds are  
322 above the estimated detection limit (3 times STDs of the backgrounds) for both filter types (87% and 87% of  
323 CHOX peaks for both 24-h Quartz and Teflon filters, OA loadings of  $1.2 \mu\text{g}/3.1 \times 10^{-2} \text{cm}^2$  (2 mm punch)). For the  
324 12-h samples (OA loadings of  $0.58 \mu\text{g}/3.1 \times 10^{-2} \text{cm}^2$  (2 mm punch)), 84% and 70% of CHOX compounds were  
325 above the detection limit for Quartz and Teflon filters, respectively (Fig. S7). Evidently, this varies for different  
326 filter loadings and punch areas.

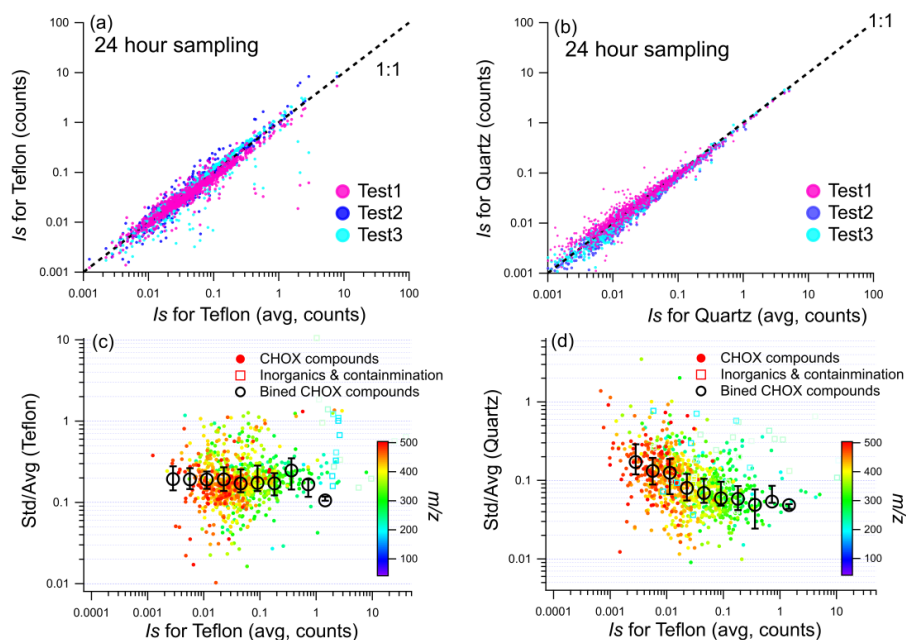
### 327 3.2 Reproducibility of signal

328 We performed reproducibility tests using three 2-mm punches from the same 24-h and 2.5-h samples of both  
329 Teflon and Quartz filters and checked the signal response with the non-uniform temperature ramping procedure.  
330 The comparisons of the blank-subtracted CHOX  $I_s$  for the 24-h and 2.5-h sample punches for both filter types are  
331 displayed in Fig. 4 and Fig. S8, respectively.

332 In Figs. 4a and 4b, we plotted the compounds' signal from one punch versus their average signal from all 3  
333 punches for the Teflon and Quartz filters, respectively. We observe a high correlation between the individual and  
334 average signals (Spearman correlation coefficients  $R_{\text{sp}}$  are 0.95–0.96 and 0.97–0.99 for Teflon and Quartz filters,



335 respectively). For each CHOX compound, we also computed the relative error (standard deviation/average signals  
336 ( $\text{Std}(I_s)/\text{Avg}(I_s)$  for the three punches) versus the average signal (Figs. 4c, 4d). The relative error for a CHOX  
337 compound was 9% for Quartz and 18% for Teflon (median relative errors) for 24-h samples (Figs. 4c, 4d). The  
338 relative error decreased with higher signal intensities (Figs. 4c, 4d), especially for the Quartz filters, suggesting  
339 that abundant compounds are measured more precisely than less abundant compounds. This trend is less apparent  
340 for Teflon filters, which is likely caused by less reproducibility for high  $I_s$  compounds. Possible explanations could  
341 be uneven distribution of particulate mass on the filter or larger uncertainties in the punching process for Teflon  
342 filters due to the extension of the material. 86% and 94% of all CHOX compounds for Teflon and Quartz filters,  
343 respectively, had  $>3$  times higher signals than the variability from the duplicate tests (Fig. S7). For the 2.5-h filter  
344 samples (Fig. S8), the relative error is higher compared to the 24-h samples (25% for Quartz, and 31% for Teflon).  
345 This is likely due to the lower OA loadings ( $9.1 \times 10^{-2} \mu\text{g}/\text{punch}$ ) of the 2.5-h sample compared to the 24-h sample  
346 ( $1.2 \mu\text{g}/\text{punch}$ ), which leads to higher uncertainties for blank subtraction and peak fitting. Still, the analytical  
347 reproducibility is acceptable, even for samples with OA loadings as low as  $\sim 0.1 \mu\text{g}$ . The relative error between  
348 repeats reported here is slightly larger ( $\sim 9\%$  and  $18\%$  for  $\sim 1 \mu\text{g}$  OA/punch for Quartz and Teflon filters, and  $25\%$   
349 for Quartz,  $31\%$  for Teflon for  $\sim 0.1 \mu\text{g}$  OA/punch) compared to the variability in signal for online FIGAERO-  
350 CIMS (5–10% for  $1 \mu\text{g}$  OA, (Lopez-Hilfiker et al., 2014)).



351

352 **Figure 4.** Comparison of the integrated signals from duplicate tests of the same 24-h sample for (a) Teflon and (b) Quartz  
353 fiber filters. The relative error ( $I_s$  ratio of standard deviation/average) value of the 3 duplicate tests as a function of  $I_s$  for (c)  
354 Teflon and (d) Quartz filters. In (c) and (d), CHOX compounds are shown as dots, inorganics as well as contaminants as  
355 squares colored by the  $m/z$ . The black cycles in (c) and (d) represent median values of signal intensity bins (with log  $I_s$  intervals  
356 of 0.3 for the  $I_s$  range of 0 to 2) and error bars represent the 25th and 75th percentile of binned values of  $\text{Std}(I_s)/\text{Avg}(I_s)$  for  
357 CHOX.

### 358 3.3 Comparison of signal for different temperature ramping protocols

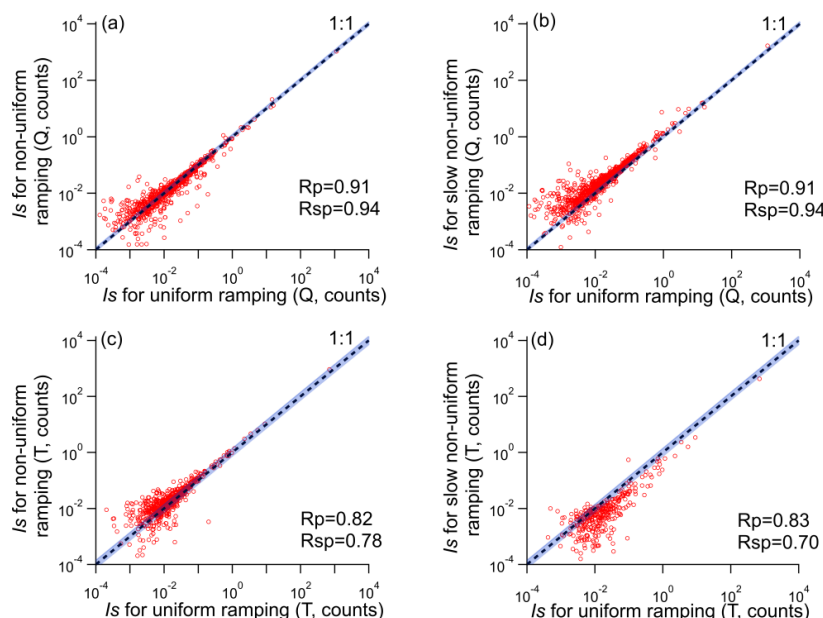
359 Here we compare the signal from different ramping protocols for the punches from the same 24-h Quartz and  
360 Teflon filters (Table 1). Since as suggested in the section 2.2.2, the  $I_s$  were calculated by the integration of the



361 normalized signals (normalized to the primary ion ( $I^-$ )), which to some extent compensates for reagent ion  
362 depletion. The signal of the field blanks is largely dominated by instrument background (i.e. there is no distinct  
363 peak in the thermogram (Fig. S1e) thus the  $I_s$  of the field blanks is highly influenced by integration time. Since  
364 the field blanks were only analyzed with non-uniform ramping, the  $I_s$  for slow non-uniform and uniform ramping  
365 protocols were assumed as the  $I_s$  of non-uniform scaled by their integration time ratios.

366 The comparison of the background-subtracted  $I_s$  of all identified compounds from different ramping protocols  
367 for a pair of 24-h Quartz and Teflon filters each is shown in Fig. 5. Since the integrated signals of the compounds  
368 within a mass spectrum are log-normally distributed (shown in Fig. S9a and 9b), a linear fit would be strongly  
369 biased by high-signal compounds such as  $\text{HNO}_3\text{I}^-$  or  $\text{C}_6\text{H}_{10}\text{O}_5\text{I}^-$ . Thus, we calculated the correlation coefficients of  
370 the log-transformed signal intensities in the comparison. The Pearson correlation coefficients ( $R_p$ ) and Spearman  
371 correlation coefficients ( $R_{sp}$ ) are as follows: for Quartz filters  $R_p = 0.91$ ,  $R_{sp} = 0.94$  for non-uniform vs uniform,  
372 and  $R_p = 0.91$ ,  $R_{sp} = 0.94$  for slow non-uniform vs uniform, and for Teflon filters  $R_p = 0.82$ ,  $R_{sp} = 0.78$  for non-  
373 uniform vs uniform, and  $R_p = 0.83$ ,  $R_{sp} = 0.70$  for slow non-uniform vs uniform protocols.

374 These numbers suggest that the Quartz samples were less affected by different temperature ramping protocols  
375 than the Teflon samples. We also note that Teflon samples exhibited lower reproducibility than Quartz samples  
376 (see section 3.2). The lowest  $R_p$  and  $R_{sp}$  were observed for the comparison between the slow non-uniform ramping  
377 and the uniform ramping procedure for Teflon filters (Fig. 5d). Possible explanations could be the higher  
378 background and thus lower signal-to-noise ratios for Teflon filters in the low ramping rate region ( $1.3\text{ }^\circ\text{C min}^{-1}$   
379 for the range of  $60\text{ }^\circ\text{C}$  to  $105\text{ }^\circ\text{C}$ ) of the slow non-uniform ramping protocol. Thus, care needs to be taken when using  
380 very slow heating rates and backgrounds need to be carefully assessed, especially for Teflon filters.



381

382 **Figure 5.** Comparison of  $I_s$  from the different temperature ramping protocols of the 24-h Quartz (Q) and Teflon (T) filter  
383 samples, (a) non-uniform and uniform ramping (Quartz sample), (b) slow non-uniform and uniform ramping (Quartz sample),  
384 (c) non-uniform and uniform ramping (Teflon sample), (d) slow non-uniform and uniform ramping (Teflon sample). The blue  
385 shaded areas represent the relative error of signal assessed in the reproducibility tests of the 24-h samples (18% for Teflon  
386 and 9% for Quartz filters). The upper and lower limits for the reproducibility-based variation are calculated as  $(1+18\%)/(1-$

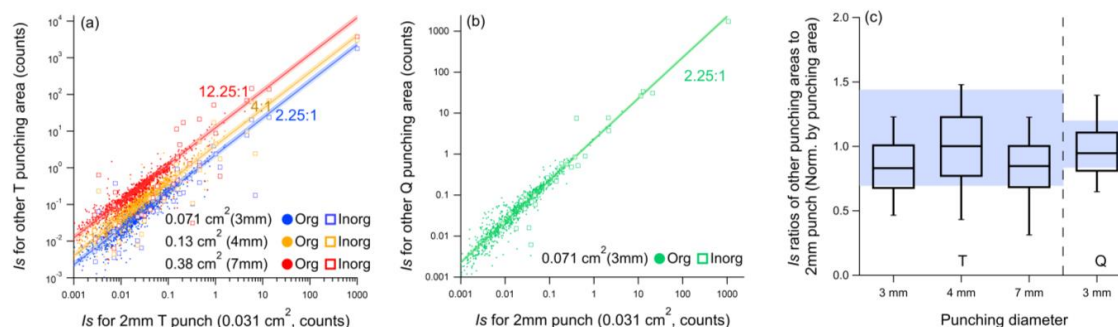


387 18%) and  $(1-18\%)/(1+18\%)$ , respectively. The upper and lower limits for the  $I_s$  distribution of Quartz caused by  
388 reproducibility are calculated as  $(1+9\%)/(1-9\%)$  and  $(1-9\%)/(1+9\%)$ , respectively.

389 For further analyses, we use the results from the non-uniform temperature ramping protocol, which represents a  
390 good balance between the influence of background due to low signal-to-noise ratios, and I<sup>-</sup> depletion. The good  
391 agreement between offline FIGAERO-CIMS and ToF-ACSM discussed in Section 3.5 further implies that such a  
392 ramping protocol is suitable for the OA loadings observed in our study.

### 393 3.4 Linearity of signal response

394 To assess the linearity of signal response to the amount of sample collected on the filter, we used punches with  
395 varying areas from one single filter. We used punch diameters of 2, 3, 4, and 7 mm for a Teflon filter and 2 mm  
396 and 3 mm for a Quartz filter. The analytical protocol was kept constant between the individual sample punches  
397 (non-uniform ramping protocol and method 2b for background subtraction). The mass loadings of the analyzed  
398 filter punches ranged from 1.2 to 15  $\mu\text{g}$  OA (2.2 to 27  $\mu\text{g}$   $\text{PM}_{2.5}$ ) for the Teflon filter and from 1.2 to 2.7  $\mu\text{g}$  OA  
399 (2.2 to 5.0  $\mu\text{g}$   $\text{PM}_{2.5}$ ) for the Quartz filter (Table 1). The blank-subtracted  $I_s$  from the different punching areas for  
400 the Quartz and Teflon filters is shown in Fig. 6. Overall, the offline FIGAERO-CIMS approach responds linearly  
401 to changes in filter mass loadings. The integrated signal ratios of CHO<sub>x</sub> are consistent with their respective area  
402 ratios (Figs. 6a, 6b), within uncertainty. In Fig. 6c we also plot the signal ratios of the 2 mm punch to the other  
403 punches, normalized by punching area (where 1 signifies perfect linearity). These ratios are generally in the range  
404 of possible variability caused by the relative error from the reproducibility tests.  
405



406

407 **Figure 6.** Comparison of the  $I_s$  between signals from punches (a) with 3 mm, 4 mm, 7 mm, and 2 mm in diameter for the same Teflon filter, and (b) with 3mm and 2 mm in diameter for the same Quartz filter. The lines in (a) and (b) represent the  
408 punching area ratios. The shaded areas in (a) and (b) represent the area ratio plus/minus the relative errors (9% for Quartz,  
409 18% for Teflon) from the reproducibility tests. (c) Distribution of  $I_s$  ratios normalized by the punching area ratios (3 mm, 4  
410 mm, and 7 mm to 2 mm diameter punches for Teflon, 3 mm to 2 mm diameter punches for Quartz). Within each box, the  
411 median (middle horizontal line), 25<sup>th</sup> and 75<sup>th</sup> percentiles (lower and upper ends of the box), and 10<sup>th</sup> and 90<sup>th</sup> percentiles  
412 (lower and upper whiskers) are shown. The shaded area in (c) represents the possible distribution of the  $I_s$  ratios due to the  
413 relative error established from the 24-h sample reproducibility tests (18% for Teflon and 9% for Quartz filters). The upper  
414 and lower limits for the Teflon  $I_s$  ratio distribution are calculated as  $(1+18\%)/(1-18\%)$  and  $(1-18\%)/(1+18\%)$ , respectively.  
415 The upper and lower limits for the Quartz  $I_s$  ratio distribution are calculated as  $(1+9\%)/(1-9\%)$  and  $(1-9\%)/(1+9\%)$ ,  
416 respectively.  
417

418 For compounds with very high signals, the response  $I_s$  ratio can deviate from the punch area ratio, not least also  
419 due to the varying degree of reagent ion depletion. The highest I<sup>-</sup> depletions were ~35%, ~60%, ~68%, and ~70%  
420 for 2mm, 3mm, 4mm, and 7mm punches, respectively. For e.g. the highest inorganic ( $\text{HNO}_3\text{I}^-$ ) and organic  
421 ( $\text{C}_6\text{H}_{10}\text{O}_5\text{I}^-$ ) ions, the  $I_s$  from a 7mm punch is only 30% and 67%, respectively, of what would be expected based  
422 on punching area ratios (7mm to 2mm). For smaller punches (4 mm/3 mm), 75%/80% and 105%/107% of the



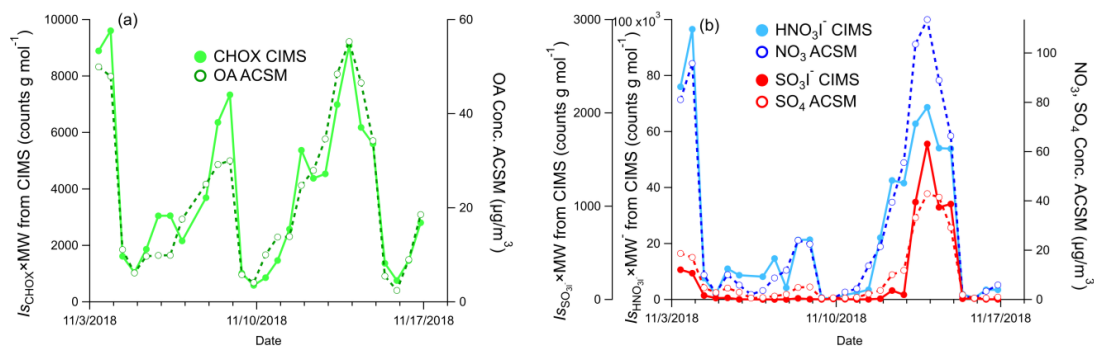
423 expected  $\text{HNO}_3\text{I}^-$  and  $\text{C}_6\text{H}_{10}\text{O}_5\text{I}^-$  signals, respectively, are detected. This indicates that for reduced amounts of  
424 desorbing material provided by smaller filter fractions, the amount of reagent ion is sufficient during the whole  
425 ramping process (lowest  $\text{I}^-/\text{C}_6\text{H}_{10}\text{O}_5\text{I}^-$  signal ratio:  $\sim 10^3$ ). In other words, if titration of reagent ion can be avoided  
426 as much as possible (e.g.  $\text{I}^-/\text{target ion}$  signal ratio:  $\sim 10^3$ ) the  $I_s$  responds linearly to concentration changes. In this  
427 study, titration is non-apparent for OA loadings of  $< 5 \mu\text{g}$  and  $I^-$  signals of  $\sim 1$  million. Therefore, it is recommended  
428 to calculate OA loadings of the samples prior analysis to determine the punching sizes in offline FIGAERO-CIMS  
429 analysis.

### 430 3.5 Comparison between offline FIGAERO-CIMS and in-situ ToF-ACSM

431 In the following, we compare the time series of the signals from offline FIGAERO-CIMS from Quartz filters and  
432 the corresponding chemical components from online ToF-ACSM measurement. The comparison between the total  
433 signal of all identified CHOX compounds and OA concentrations from the ToF-ACSM is displayed in Fig.7a.  
434 Here, the FIGAERO-CIMS signals of five polyols ( $\text{C}_8\text{H}_{18}\text{O}_5\text{I}^-$ ,  $\text{C}_{10}\text{H}_{22}\text{O}_6\text{I}^-$ ,  $\text{C}_{12}\text{H}_{26}\text{O}_7\text{I}^-$ ,  $\text{C}_{14}\text{H}_{30}\text{O}_8\text{I}^-$ ,  $\text{C}_{16}\text{H}_{34}\text{O}_9\text{I}^-$ )  
435 were excluded, which were contaminants from the lab due to their inexplicably high  $I_s$  in 3 of the 27 12-h samples  
436 and the usage of diethylene glycol (DEG) in the lab. Even though  $\text{I}^-$  is selective towards oxygenated organic  
437 compounds, the total CHOX signal measured by offline FIGAERO-CIMS in this study highly correlates with OA  
438 measured by the ToF-ACSM ( $R_p = 0.94$ ), which is known to be dominated by secondary organic aerosols (SOA)  
439 (Cai et al., 2020; Kulmala et al., 2021; Jia et al., 2008).

440 The time series of the 12h- $I_s$  for  $\text{HNO}_3\text{I}^-$  and  $\text{SO}_3\text{I}^-$  measured by offline FIGAERO-CIMS correlate well with the  
441  $\text{NO}_3$  and  $\text{SO}_4$  concentrations from ToF-ACSM ( $R_p = 0.94$  and  $0.95$ , Fig. 7b). The signal of  $\text{HNO}_3\text{I}^-$  in the particle  
442 phase measured by FIGAERO-CIMS is as an indicator of particulate nitrate and organonitrate (Lee et al., 2016),  
443 and the signal of  $\text{SO}_3\text{I}^-$  is related to inorganic sulfate and sulfur-containing organics (Ye et al., 2021; Cao et al.,  
444 2019). A similarly good correlation is observed between the signal intensity from the same offline FIGAERO-  
445 CIMS method and  $\text{PM}_{2.5}$  component concentrations measured in-situ by ToF-ACSM in a previous study conducted  
446 in Beijing at Peking University campus (Zheng et al., 2021), which is shown in Fig. S10 (Zheng et al., 2021). The  
447 generally good temporal correlation of different PM constituents between offline FIGAERO-CIMS and ToF-  
448 ACSM analyses highlights the good performance of the offline FIGAERO-CIMS method, at least in terms of bulk  
449 PM constituents.

450



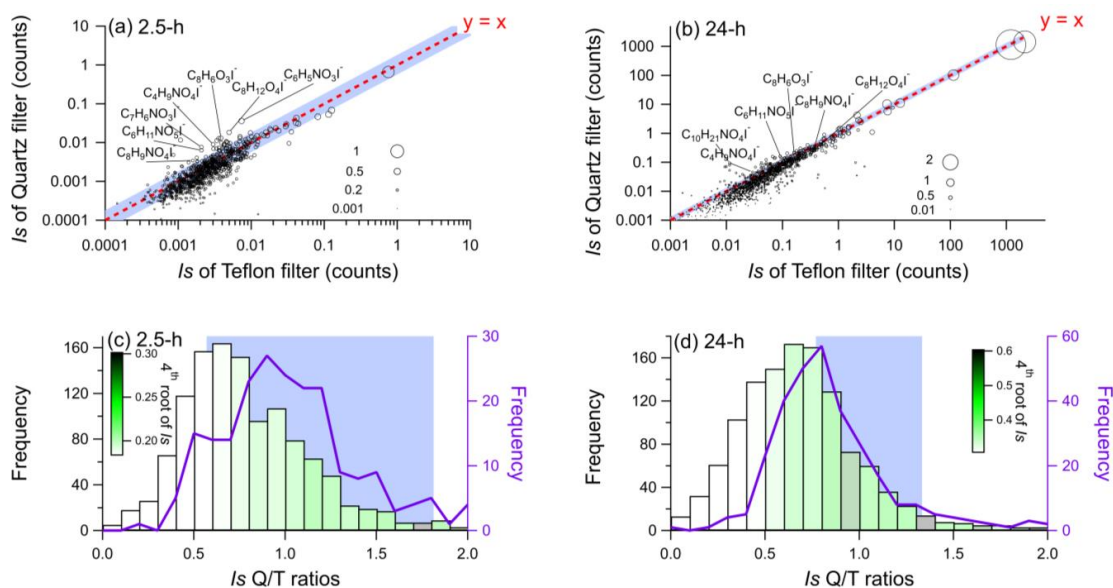
451

452 **Figure 7.** Comparison of the time series of the integrated signals of inorganic and organic compounds from 12-h samples (2  
453 mm punches) analyzed by offline FIGAERO-CIMS, and chemical components measured in-situ by ToF-ACSM, (a) total  
454 CHOX from FIGAERO-CIMS and OA from ToF-ACSM, (b)  $\text{HNO}_3\text{I}^-$  from FIGAERO-CIMS and  $\text{NO}_3$  from ToF-ACSM,  
455 (c)  $\text{SO}_3\text{I}^-$  from FIGAERO-CIMS and  $\text{SO}_4$  from ToF-ACSM. To compare with the  $\text{PM}_{2.5}$  component concentrations from the  
456 ToF-ACSM, the  $I_s$  of each compound from FIGAERO-CIMS was multiplied by their molecular weight (MW) in (a) and (b).



### 3.6 Comparison of Quartz and Teflon filters

In the following, we compare the  $I_s$  from simultaneously collected Quartz and Teflon filter samples (collection times 2.5 h, 12 h, and 24 h, see Table 1). Fig. 8a and b show the comparison of the average  $I_s$  of compounds (3 samples each) for both filter types, with 2.5h (OA loading of  $9.1 \times 10^{-2} \mu\text{g}$ ) and 24h (OA loading of  $1.2 \mu\text{g}$ ) collection times. The mass spectra show an overall similar pattern, we observe a non-negligible difference, especially for the 2.5h samples (Fig. 8a). The log-transformed signals from Quartz and Teflon samples correlate better for 24-h samples ( $R_p = 0.96$ ,  $R_{sp} = 0.95$ , Fig. S9c) than for the 2.5-h samples ( $R_p = 0.88$ ,  $R_{sp} = 0.87$ , Fig. S9d). In addition, the signal observed for Quartz filter samples is generally slightly lower than for Teflon filter samples (Fig. 8c, d). Compounds with high Quartz/Teflon-signal ratios are in general semi- or low volatile compounds (operationally defined as having a  $T_{\text{max}} < 60^\circ\text{C}$ ). These compounds tend to be in the CHO and especially CHON category and exhibit a higher degree of unsaturation (e.g.  $\text{C}_8\text{H}_6\text{O}_3\text{I}^-$ ,  $\text{C}_6\text{H}_5\text{NO}_3\text{I}^-$  and  $\text{C}_7\text{H}_6\text{NO}_3\text{I}^-$ ). They can be aromatics or their thermal fragmentation products (Liu et al., 2019). Due to the high surface area of the Quartz filters, semi- or low volatile compounds are more easily adsorbed than on Teflon filters, potentially resulting in higher positive artefacts. Compounds with low Quartz/Teflon-signal ratios tend to have overall low signal. Despite the application of a blank determination method that takes instrument backgrounds into account (Method 2b), higher residuals were still observed for the lower signal compounds, especially for the Teflon filters (as seen also for the 2.5-h and 0.5-h sample comparison (Fig. 3d). In contrast, compounds with a higher signal tend to be in the range of Q/T ratios expected based on the observed variability from the reproducibility tests (shown in Fig. 8c and 8d).



476

**Figure 8.** Comparison of the integrated signal intensities of all identified compounds for the Quartz fiber and Teflon filter samples, (a) 2.5-h samples, (b) 24-h samples. The size of symbols in (a) and (b) is proportional to the 4<sup>th</sup> root of the signal intensity of each compound from the Quartz filter. The distribution of  $I_s$  ratios (green bars) of Quartz/Teflon, the distribution of  $I_s$  ratios (purple lines) for the 25% of compounds with the highest signal for (c) 2.5-h samples, and (d) 24-h samples. The bars in (c) and (d) are colored by the average of the 4<sup>th</sup> root of the signal intensity for the Quartz filter. The shaded area in each panel represents the possible distribution of  $I_s$  ratios of Quartz/Teflon from the relative errors from the duplicate tests of 2.5-h (25% for Quartz and 31% for Teflon) and 24-h (9% for Quartz and 18% for Teflon) samples. The upper and lower limits for the 2.5-h Quartz/Teflon  $I_s$  ratios were calculated as  $(1+25\%)/(1-31\%)$  and  $(1-25\%)/(1+31\%)$ , respectively. The upper and

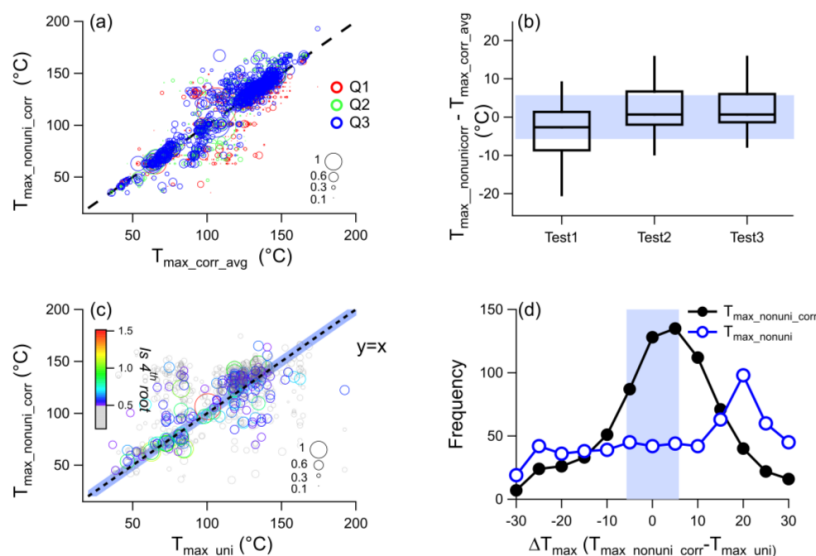


485 lower limits for the 24-h Quartz/Teflon  $I_s$  ratios were calculated as  $(1+9\%)/(1-18\%)$  and  $(1-9\%)/(1+18\%)$ , respectively. The  
486  $T_{\max}$  was corrected.

### 487 3.7 $T_{\max}$ : Influence of temperature ramping protocol and filter type

488 Non-uniform ramping of the temperature due to reagent ion titration is more likely needed when the FIGAERO-  
489 CIMS is run in offline mode compared to online mode, where sampling times and resulting filter mass loadings  
490 can be adjusted more easily. We have therefore developed a method (see section 2.2.4) to recover  $T_{\max}$  from non-  
491 uniform ramping protocols, i.e. to make it comparable to  $T_{\max}$  from uniform ramping protocols. Compared to the  
492 raw thermograms, the shape of the corrected thermograms is more similar to that of the uniform protocol (Fig. S11  
493 and S12), since the thermograms were re-gridded to the same temperature intervals ( $3^\circ\text{C}$ ).

494 Firstly, we tested the variation of  $T_{\max}$  from the three duplicate tests of the Quartz filters using the non-uniform  
495 ramping protocol and thermogram correction (Fig. 9a). After correction, the corrected  $T_{\max}$  ( $T_{\max\_nonuni\_corr}$ ) from  
496 individual tests was highly correlated with their average ( $T_{\max\_corr\_avg}$ ,  $R_p = 0.87\text{--}0.93$ ). The median value of the  
497 difference between  $T_{\max\_nonuni\_corr}$  of duplicate tests and their average for all compounds ranges from  $-2.7\text{--}0.7^\circ\text{C}$   
498 (shown in Fig.9b). The majority of compounds (52%–70%) have a  $T_{\max}$  difference within  $5^\circ\text{C}$ , close to the value  
499 reported in previously ( $\sim 2^\circ\text{C}$ , (Lopez-Hilfiker et al., 2014)). The median standard deviation of the difference  
500 between the corrected  $T_{\max}$  of individual tests ( $T_{\max\_nonuni\_corr}$ ) and their average ( $T_{\max\_corr\_avg}$ ) from all compounds  
501 is  $5.7^\circ\text{C}$ , which is defined as the variation of  $T_{\max}$  for duplicate tests.



502

503 **Figure 9.** (a) Comparison of  $T_{\max\_nonuni\_corr}$  from the 3 duplicate tests and their average ( $T_{\max\_corr\_avg}$ ), (b) distribution of the  
504 difference between the 3 triplicate tests and the  $T_{\max\_corr\_avg}$ , (c) comparison of  $T_{\max}$  from the corrected non-uniform ramping  
505 and uniform ramping protocol ( $T_{\max\_uni}$ ), (d) histogram of  $\Delta T_{\max}$  between  $T_{\max}$  from the uniform ramping protocol ( $T_{\max\_uni}$ )  
506 and non-uniform with ( $T_{\max\_nonuni\_corr}$ )/without ( $T_{\max\_nonuni}$ ) correction. The size of symbols in (a) and (b) is proportional to the  
507 4<sup>th</sup> root of the integrated signal intensity. The 4<sup>th</sup> root of the signal intensity  $<0.5$  is shown in grey. The uniform ramping  
508 protocol test and 3 duplicate non-uniform ramping protocol tests were conducted for the same 24-h Quartz filter (Nov 23 to  
509 24). The shaded area in (b), (c), and (d) represents  $T_{\max}$  variation ( $\pm 5.7^\circ\text{C}$ ) from the duplicate tests.

510 We take the uniform sampling protocol (see Fig. 1d) as the basis since this is the commonly used protocol for  
511 FIGAERO-CIMS in online mode. The comparison of  $T_{\max}$  from the corrected non-uniform and the uniform  
512 ramping protocols is shown in Fig. 9c. Generally, after correction for the non-uniform ramping, the Pearson  
513 correlation coefficient of  $T_{\max\_nonuni\_corr}$  and  $T_{\max\_uni}$  is higher ( $R_p = 0.60$ ) compared to the uncorrected ones with

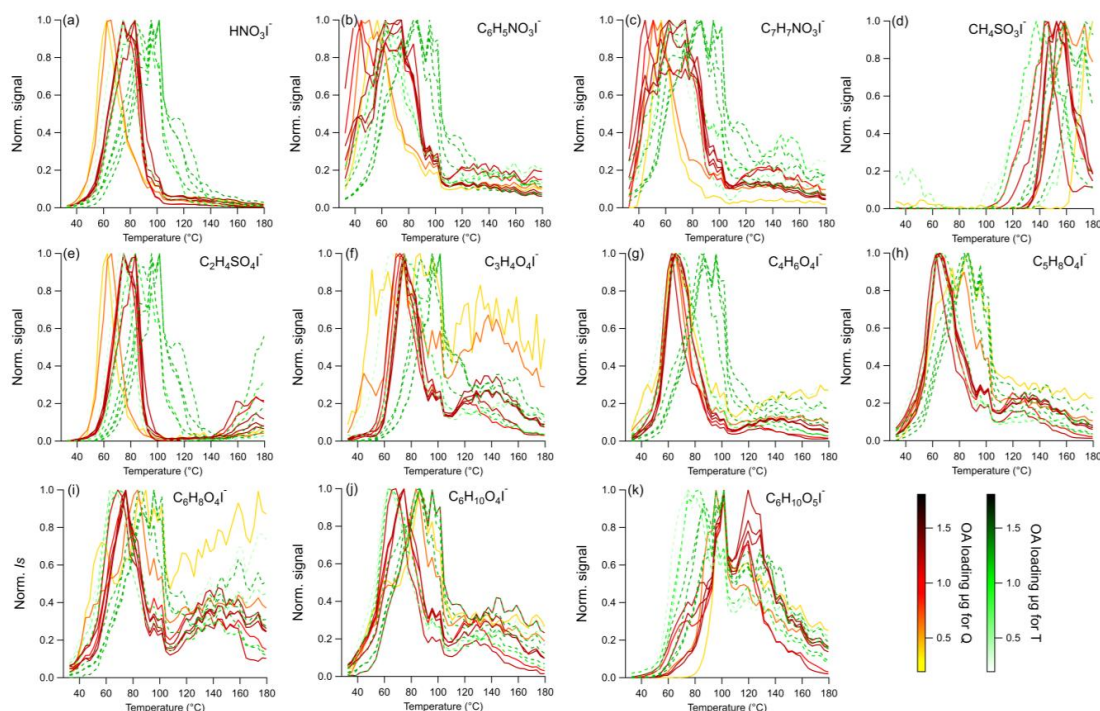




514 the uniform protocol ( $R_p = 0.20$ ,  $T_{\max\_nonuni}$  vs  $T_{\max\_uni}$ ). The correlation coefficients were even higher (0.72 and  
515 0.84) for the 400 and 100 compounds with the highest signal intensity. In Fig. 9d we plot the frequency distribution  
516 of the differences between the corrected  $T_{\max}$  ( $T_{\max\_nonuni\_corr}$ ) and  $T_{\max}$  from the uniform protocol ( $T_{\max\_uni}$ ) for each  
517 CHO compound in the spectrum. For 73% of the compounds, the difference in  $T_{\max}$  between the two ramping  
518 protocols lies between  $-15$  and  $15$  °C, and 41 % of compounds exhibit a difference of  $0 - \pm 5$  °C.

519 In the next step, we compared the volatility derived from  $T_{\max}$  for Quartz fiber and Teflon filters. We selected a  
520 number of inorganic and organic compounds, based on their high average signals for the whole sampling period,  
521 for comparison of thermograms from 12-h and 24-h Teflon and Quartz filters sampled in parallel (Table S1, Fig.  
522 10). Compounds include  $\text{HNO}_3\text{I}$ , CHON ( $\text{C}_6\text{H}_5\text{NO}_3\text{I}$ ,  $\text{C}_7\text{H}_7\text{NO}_3\text{I}$ ) and CHOS ( $\text{CH}_4\text{SO}_3\text{I}$ ,  $\text{C}_2\text{H}_4\text{SO}_4\text{I}$ ) compounds  
523 as well as CHO compounds with  $C_{\text{num}} \geq 3$  ( $\text{C}_3\text{H}_4\text{O}_4\text{I}$ ,  $\text{C}_4\text{H}_6\text{O}_4\text{I}$ ,  $\text{C}_5\text{H}_8\text{O}_4\text{I}$ ,  $\text{C}_6\text{H}_8\text{O}_4\text{I}$ ,  $\text{C}_6\text{H}_{10}\text{O}_4\text{I}$ ,  $\text{C}_6\text{H}_{10}\text{O}_5\text{I}$ ).  
524 Compounds with  $C_{\text{num}} < 3$  (e.g.  $\text{CH}_2\text{O}_2\text{I}$ ) were excluded due to possible gas-phase interference and more likely  
525 influenced by thermal decomposition. Some compounds exhibited similar thermogram shapes for the two types of  
526 filters, such as  $\text{C}_6\text{H}_{10}\text{O}_5\text{I}$  and  $\text{CH}_4\text{SO}_3\text{I}$ , while for some other species, the thermograms were different. Taking  
527  $\text{C}_3\text{H}_4\text{O}_4\text{I}$  as an example, a bimodal thermogram shape with peaks around  $100$  °C and  $150$  °C was observed for the  
528 Quartz filter, while only a unimodal peak around  $90$  °C was observed for the Teflon filter. The different  
529 thermogram shapes of individual compounds for the different filter types might warrant further investigation with  
530 a focus on the role of filter type properties (such as pore size, thickness, absorption, and hydrophobic/hydrophilic  
531 properties).

532



533

534 **Figure 10.** Normalized thermograms for Teflon (T, dashed lines) and Quartz (Q, solid lines) filters of, (a)  $\text{HNO}_3\text{I}$ , (b)  
535  $\text{C}_6\text{H}_5\text{NO}_3\text{I}$ , (c)  $\text{C}_7\text{H}_7\text{NO}_3\text{I}$ , (d)  $\text{CH}_4\text{SO}_3\text{I}$ , (e)  $\text{C}_2\text{H}_4\text{SO}_4\text{I}$ , (f)  $\text{C}_3\text{H}_4\text{O}_4\text{I}$ , (g)  $\text{C}_4\text{H}_6\text{O}_4\text{I}$ , (h)  $\text{C}_5\text{H}_8\text{O}_4\text{I}$ , (i)  $\text{C}_6\text{H}_8\text{O}_4\text{I}$ , (j)  $\text{C}_6\text{H}_{10}\text{O}_4\text{I}$ ,  
536 (k)  $\text{C}_6\text{H}_{10}\text{O}_5\text{I}$ . The thermograms were first corrected (section 2.2.4) and then normalized to signals in  $T_{\max}$  and colored by the  
537 OA mass loading. The sampling information of the thermograms presented here is listed in Table S1.



538 In addition, we found that compounds with higher mass loadings appeared to have a higher  $T_{\max}$  (e.g.  $C_2H_4SO_4I^-$   
539 and  $C_7H_7NO_3I^-$ , shown in Fig 10), consistent with previous findings using Teflon filters (Huang et al., 2018;  
540 Ylisirniö et al., 2021). The variability in  $T_{\max}$  induced by varying PM loadings is within  $5^\circ C$  for 29% of compounds,  
541 and within  $15^\circ C$  for 54% of all compounds for Quartz filters, and 35% and 57% of compounds, respectively, for  
542 Teflon samples. The  $T_{\max}$  variation due to filter type ( $R_p=0.27$ ) is much larger than the one induced by filter  
543 loadings. Thus, the direct comparison of  $T_{\max}$  between Quartz and Teflon filters is not feasible, warranting further  
544 research.

#### 545 4. Discussion

546 This study introduces methods and assesses the performance of using the FIGAERO-CIMS in offline mode, i.e.  
547 to analyze particulate matter collected temporally and locally distant from the instrument on filter samples (Quartz  
548 and Teflon). Such an approach greatly enhances the capabilities of the FIGAERO-CIMS for analyzing atmospheric  
549 samples, as it enables the probing of the air at locations where and on occasions when *in-situ* deployments are  
550 difficult.

551 Due to the difficulties in background determination for offline FIGAERO-CIMS, in this study, we propose  
552 different background determination methods, which were further assessed by the comparison between samples  
553 from 5 different 0.5-h samples and a 2.5-h sample collected in parallel. We applied non-uniform temperature  
554 ramping to avoid reagent ion titration and a background scaling method taking interference of variable instrument  
555 backgrounds into account. In general, the offline FIGAERO-CIMS approach using the methods presented in this  
556 study can be used for providing OA composition information with typical offline sampling times (e.g. 12h and  
557 24h) samples: (1) the reproducibility of integrated signal intensity is within  $\pm 20\%$  for both filter types (18% for  
558 Teflon and 9% for Quartz), (2) detected signals respond linearly to changes in the samples' mass loadings, (3) the  
559 signals of CHOX and  $SO_3I^-$ ,  $HNO_3I^-$  correlated well with corresponding  $PM_{2.5}$  chemical component concentrations  
560 of OA,  $SO_4$ , and  $NO_3$  measured by ToF-ACSM ( $R_p=0.94$  to  $0.95$ ), (4) the log-transformed mass spectra are highly  
561 correlated ( $R_p>0.9$ ) between Quartz and Teflon filters for typical offline sampling times (e.g. 12h and 24h), and  
562 for high-signal compounds the  $I_s$  ratios between Quartz and Teflon filters are generally within reproducibility  
563 variation. Overall, this highlights the possibility of using widely available and stored Quartz filters to identify  
564 CHOX molecular composition with FIGAERO-CIMS.

565  $T_{\max}$  retrieved from corrected thermograms of desorption with non-uniform ramping protocols are comparable to  
566  $T_{\max}$  from uniform ramping protocol for high signal intensity compounds ( $R_p=0.72-0.84$ ). More than 50% of  
567 compounds have  $T_{\max}$  values that are reproducible within  $5^\circ C$  for duplicate tests ( $R_p=0.87-0.93$ ) of the same  
568 sample, and for  $>50\%$  of compounds,  $T_{\max}$  varies within  $15^\circ C$  for different mass loadings. Yet,  $T_{\max}$  is strongly  
569 affected by the filter material (Teflon vs Quartz) leading to a large discrepancy in  $T_{\max}$  between Quartz and Teflon  
570 samples ( $R_p=0.27$ ), hindering direct comparisons and warranting further research.

571 In summary, using FIGAERO-CIMS to analyze offline samples is a useful and simple way to investigate OA  
572 molecular composition, but care needs to be taken for  $T_{\max}$  analyses. This opens broad applications to study OA  
573 molecular composition, sources, and formation processes at several sites simultaneously and in long-term  
574 deployments.

#### 575 Author contributions

576 JC, KR, CM, and MK designed the research. JC, FXZ, and WD collected the samples at the BUCT site. JC, CW,  
577 SH, KR, and CM analyzed the samples and interpreted the data. ZY and CQ analyzed the samples collected at  
578 the Peking University campus site. CM, KR, and MK supervised this research. JC, KR, and CM wrote the



579 manuscript with contributions from all co-authors. All authors have given approval to the final version of this  
580 manuscript.

### 581 *Acknowledgements*

582 The work is supported by the Knut and Alice Wallenberg Foundation (WAF project CLOUDFORM, grant no.  
583 2017.0165), the Academy of Finland (Center of Excellence in Atmospheric Sciences, project no. 307331, and  
584 PROFI3 funding, 311932, ACCC Flagship 337549), the European Research Council via ATM-GTP (742206),  
585 Wihuri Foundation, and the Jane and Aatos Erkkö Foundation. KRD acknowledges support by the SNF mobility  
586 grant P2EZP2\_181599. The authors also would like to thank Federico Bianchi's kind help and suggestions as well  
587 as the effort from all the researchers in the BUCT project to maintain the BUCT site.

588

### 589 **Reference**

- 590 Bannan, T. J., Le Breton, M., Priestley, M., Worrall, S. D., Bacak, A., Marsden, N. A., Merha, A., Hammes, J.,  
591 Hallquist, M., Alfarra, M. R., Krieger, U. K., Reid, J. P., Jayne, J., Robinson, W., McFiggans, G., Coe, H., Percival,  
592 C. J., and Topping, D.: A method for extracting calibrated volatility information from the FIGAERO-HR-ToF-  
593 CIMS and its application to chamber and field studies, *Atmospheric Measurement Techniques Discussions*, 1-12,  
594 10.5194/amt-2018-255, 2018.
- 595 Cai, J., Wu, C., Wang, J., Du, W., Zheng, F., Hakala, S., Fan, X., Chu, B., Yao, L., Feng, Z., Liu, Y., Sun, Y.,  
596 Zheng, J., Yan, C., Bianchi, F., Kulmala, M., Mohr, C., and Daellenbach, K. R.: Influence of organic aerosol  
597 molecular composition on particle absorptive properties in autumn Beijing, *Atmospheric Chemistry and Physics*,  
598 22, 1251-1269, 10.5194/acp-22-1251-2022, 2022.
- 599 Cai, J., Chu, B., Yao, L., Yan, C., Heikkinen, L. M., Zheng, F., Li, C., Fan, X., Zhang, S., Yang, D., Wang, Y.,  
600 Kokkonen, T. V., Chan, T., Zhou, Y., Dada, L., Liu, Y., He, H., Paasonen, P., Kujansuu, J. T., Petäjä, T., Mohr,  
601 C., Kangasluoma, J., Bianchi, F., Sun, Y., Croteau, P. L., Worsnop, D. R., Kerminen, V.-M., Du, W., Kulmala,  
602 M., and Daellenbach, K. R.: Size-segregated particle number and mass concentrations from different emission  
603 sources in urban Beijing, *Atmospheric Chemistry and Physics*, 20, 12721-12740, 10.5194/acp-20-12721-2020,  
604 2020.
- 605 Cao, L. M., Huang, X. F., Wang, C., Zhu, Q., and He, L. Y.: Characterization of submicron aerosol volatility in  
606 the regional atmosphere in Southern China, *Chemosphere*, 236, 124383, 10.1016/j.chemosphere.2019.124383,  
607 2019.
- 608 Cappa, C. D., Onasch, T. B., Massoli, P., Worsnop, D. R., Bates, T. S., Cross, E. S., Davidovits, P., Hakala, J.,  
609 Hayden, K. L., Jobson, B. T., Kolesar, K. R., Lack, D. A., Lerner, B. M., Li, S.-M., Mellon, D., Nuaaman, I.,  
610 Olfert, J. S., Petäjä, T., Quinn, P. K., Song, C., Subramanian, R., Williams, E. J., and Zaveri, R. A.: Radiative  
611 Absorption Enhancements Due to the Mixing State of Atmospheric Black Carbon, *Science*, 337, 1078-1081, 2012.
- 612 Daellenbach, K. R., Uzu, G., Jiang, J., Cassagnes, L. E., Leni, Z., Vlachou, A., Stefenelli, G., Canonaco, F., Weber,  
613 S., Segers, A., Kuenen, J. J. P., Schaap, M., Favez, O., Albinet, A., Aksoyoglu, S., Dommen, J., Baltensperger, U.,  
614 Geiser, M., El Haddad, I., Jaffrezo, J. L., and Prevot, A. S. H.: Sources of particulate-matter air pollution and its  
615 oxidative potential in Europe, *Nature*, 587, 414-419, 10.1038/s41586-020-2902-8, 2020.
- 616 Fan, X., Cai, J., Yan, C., Zhao, J., Guo, Y., Li, C., Dällenbach, K. R., Zheng, F., Lin, Z., Chu, B., Wang, Y., Dada,  
617 L., Zha, Q., Du, W., Kontkanen, J., Kurtén, T., Iyer, S., Kujansuu, J. T., Petäjä, T., Worsnop, D. R., Kerminen,  
618 V.-M., Liu, Y., Bianchi, F., Tham, Y. J., Yao, L., and Kulmala, M.: Atmospheric gaseous hydrochloric and  
619 hydrobromic acid in urban Beijing, China: detection, source identification and potential atmospheric impacts,  
620 *Atmospheric Chemistry and Physics*, 21, 11437-11452, 10.5194/acp-21-11437-2021, 2021.
- 621 Farmer, D. K., Vance, M. E., Abbatt, J. P. D., Abeleira, A., Alves, M. R., Arata, C., Boedicker, E., Bourne, S.,  
622 Cardoso-Saldana, F., Corsi, R., DeCarlo, P. F., Goldstein, A. H., Grassian, V. H., Hildebrandt Ruiz, L., Jimenez,  
623 J. L., Kahan, T. F., Katz, E. F., Mattila, J. M., Nazaroff, W. W., Novoselac, A., O'Brien, R. E., Or, V. W., Patel,



- 624 S., Sankhyan, S., Stevens, P. S., Tian, Y., Wade, M., Wang, C., Zhou, S., and Zhou, Y.: Overview of HOMEChem:  
625 House Observations of Microbial and Environmental Chemistry, *Environ Sci Process Impacts*, 21, 1280-1300,  
626 10.1039/c9em00228f, 2019.
- 627 Guo, Y., Yan, C., Li, C., Ma, W., Feng, Z., Zhou, Y., Lin, Z., Dada, L., Stolzenburg, D., Yin, R., Kontkanen, J.,  
628 Daellenbach, K. R., Kangasluoma, J., Yao, L., Chu, B., Wang, Y., Cai, R., Bianchi, F., Liu, Y., and Kulmala, M.:  
629 Formation of nighttime sulfuric acid from the ozonolysis of alkenes in Beijing, *Atmospheric Chemistry and  
630 Physics*, 21, 5499-5511, 10.5194/acp-21-5499-2021, 2021.
- 631 Gustafson, K. E. and Dickhut, R. M.: Particle/Gas Concentrations and Distributions of PAHs in the Atmosphere  
632 of Southern Chesapeake Bay, *Environmental Science & Technology*, 31, 140-147, 10.1021/es9602197, 1997.
- 633 Huang, R. J., Zhang, Y., Bozzetti, C., Ho, K. F., Cao, J. J., Han, Y., Daellenbach, K. R., Slowik, J. G., Platt, S. M.,  
634 Canonaco, F., Zotter, P., Wolf, R., Pieber, S. M., Bruns, E. A., Crippa, M., Ciarelli, G., Piazzalunga, A.,  
635 Schwikowski, M., Abbaszade, G., Schnelle-Kreis, J., Zimmermann, R., An, Z., Szidat, S., Baltensperger, U., El  
636 Haddad, I., and Prevot, A. S.: High secondary aerosol contribution to particulate pollution during haze events in  
637 China, *Nature*, 514, 218-222, 10.1038/nature13774, 2014.
- 638 Huang, W., Saathoff, H., Shen, X., Ramisetty, R., Leisner, T., and Mohr, C.: Seasonal characteristics of organic  
639 aerosol chemical composition and volatility in Stuttgart, Germany, *Atmospheric Chemistry and Physics*, 19,  
640 11687-11700, 10.5194/acp-19-11687-2019, 2019a.
- 641 Huang, W., Saathoff, H., Shen, X., Ramisetty, R., Leisner, T., and Mohr, C.: Chemical Characterization of Highly  
642 Functionalized Organonitrates Contributing to Night-Time Organic Aerosol Mass Loadings and Particle Growth,  
643 *Environ Sci Technol*, 53, 1165-1174, 10.1021/acs.est.8b05826, 2019b.
- 644 Huang, W., Saathoff, H., Pajunoja, A., Shen, X., Naumann, K.-H., Wagner, R., Virtanen, A., Leisner, T., and  
645 Mohr, C.: &lt;i>Pinene secondary organic aerosol at low temperature: chemical composition and  
646 implications for particle viscosity, Atmospheric Chemistry and Physics, 18, 2883-2898, 10.5194/acp-18-2883-  
647 2018, 2018.
- 648 Jia, Y., Rahn, K. A., He, K., Wen, T., and Wang, Y.: A novel technique for quantifying the regional component  
649 of urban aerosol solely from its sawtooth cycles, *Journal of Geophysical Research*, 113, 10.1029/2008jd010389,  
650 2008.
- 651 Kontkanen, J., Deng, C., Fu, Y., Dada, L., Zhou, Y., Cai, J., Dällenbach, K. R., Hakala, S., Kokkonen, T. V., Lin,  
652 Z., Liu, Y., Wang, Y., Yan, C., Petäjä, T., Jiang, J., Kulmala, M., and Paasonen, P., 10.5194/acp-2020-215, 2020.
- 653 Koss, A. R., Sekimoto, K., Gilman, J. B., Selimovic, V., Coggon, M. M., Zarzana, K. J., Yuan, B., Lerner, B. M.,  
654 Brown, S. S., Jimenez, J. L., Krechmer, J., Roberts, J. M., Warneke, C., Yokelson, R. J., and de Gouw, J.: Non-  
655 methane organic gas emissions from biomass burning: identification, quantification, and emission factors from  
656 PTR-ToF during the FIREX 2016 laboratory experiment, *Atmospheric Chemistry and Physics*, 18, 3299-3319,  
657 10.5194/acp-18-3299-2018, 2018.
- 658 Kulmala, M., Dada, L., Daellenbach, K. R., Yan, C., Stolzenburg, D., Kontkanen, J., Ezhova, E., Hakala, S.,  
659 Tuovinen, S., Kokkonen, T. V., Kurppa, M., Cai, R., Zhou, Y., Yin, R., Baalbaki, R., Chan, T., Chu, B., Deng, C.,  
660 Fu, Y., Ge, M., He, H., Heikkinen, L., Junninen, H., Liu, Y., Lu, Y., Nie, W., Rusanen, A., Vakkari, V., Wang, Y.,  
661 Yang, G., Yao, L., Zheng, J., Kujansuu, J., Kangasluoma, J., Petaja, T., Paasonen, P., Jarvi, L., Worsnop, D., Ding,  
662 A., Liu, Y., Wang, L., Jiang, J., Bianchi, F., and Kerminen, V. M.: Is reducing new particle formation a plausible  
663 solution to mitigate particulate air pollution in Beijing and other Chinese megacities?, *Faraday Discuss*, 226, 334-  
664 347, 10.1039/d0fd00078g, 2021.
- 665 Le Breton, M., Psichoudaki, M., Hallquist, M., Watne, Å. K., Lutz, A., and Hallquist, Å. M.: Application of a  
666 FIGAERO ToF CIMS for on-line characterization of real-world fresh and aged particle emissions from buses,  
667 *Aerosol Science and Technology*, 53, 244-259, 10.1080/02786826.2019.1566592, 2019.
- 668 Lee, B. H., Lopez-Hilfiker, F. D., amp, apos, Ambro, E. L., Zhou, P., Boy, M., Petäjä, T., Hao, L., Virtanen, A.,  
669 and Thornton, J. A.: Semi-volatile and highly oxygenated gaseous and particulate organic compounds observed  
670 above a boreal forest canopy, *Atmospheric Chemistry and Physics*, 18, 11547-11562, 10.5194/acp-18-11547-2018,  
671 2018.
- 672 Lee, B. H., Mohr, C., Lopez-Hilfiker, F. D., Lutz, A., Hallquist, M., Lee, L., Romer, P., Cohen, R. C., Iyer, S.,  
673 Kurten, T., Hu, W., Day, D. A., Campuzano-Jost, P., Jimenez, J. L., Xu, L., Ng, N. L., Guo, H., Weber, R. J., Wild,  
674 R. J., Brown, S. S., Koss, A., de Gouw, J., Olson, K., Goldstein, A. H., Seco, R., Kim, S., McAvey, K., Shepson,



- 675 P. B., Starn, T., Baumann, K., Edgerton, E. S., Liu, J., Shilling, J. E., Miller, D. O., Brune, W., Schobesberger, S.,  
676 D'Ambro, E. L., and Thornton, J. A.: Highly functionalized organic nitrates in the southeast United States:  
677 Contribution to secondary organic aerosol and reactive nitrogen budgets, *Proc Natl Acad Sci U S A*, 113, 1516-  
678 1521, 10.1073/pnas.1508108113, 2016.
- 679 Liu, L., Rao, Z., Wang, Y., Arandiyani, H., Gong, J., Liang, M., and Guo, F.: Characteristics and Health Risk  
680 Assessment of Semi-Volatile Organic Contaminants in Rural Pond Water of Hebei Province, *Int J Environ Res*  
681 *Public Health*, 16, 10.3390/ijerph16224481, 2019.
- 682 Liu, Q., Baumgartner, J., Zhang, Y., and Schauer, J. J.: Source apportionment of Beijing air pollution during a  
683 severe winter haze event and associated pro-inflammatory responses in lung epithelial cells, *Atmospheric*  
684 *Environment*, 126, 28-35, <https://doi.org/10.1016/j.atmosenv.2015.11.031>, 2016.
- 685 Liu, Y., Zhang, Y., Lian, C., Yan, C., Feng, Z., Zheng, F., Fan, X., Chen, Y., Wang, W., Chu, B., Wang, Y., Cai,  
686 J., Du, W., Daellenbach, K. R., Kangasluoma, J., Bianchi, F., Kujansuu, J., Petäjä, T., Wang, X., Hu, B., Wang,  
687 Y., Ge, M., He, H., and Kulmala, M.: The promotion effect of nitrous acid on aerosol formation in wintertime in  
688 Beijing: the possible contribution of traffic-related emissions, *Atmospheric Chemistry and Physics*, 20, 13023-  
689 13040, 10.5194/acp-20-13023-2020, 2020.
- 690 Lopez-Hilfiker, F. D., Pospisilova, V., Huang, W., Kalberer, M., Mohr, C., Stefenelli, G., Thornton, J. A.,  
691 Baltensperger, U., Prevot, A. S. H., and Slowik, J. G.: An extractive electrospray ionization time-of-flight mass  
692 spectrometer (EESI-TOF) for online measurement of atmospheric aerosol particles, *Atmospheric Measurement*  
693 *Techniques*, 12, 4867-4886, 10.5194/amt-12-4867-2019, 2019.
- 694 Lopez-Hilfiker, F. D., Mohr, C., Ehn, M., Rubach, F., Kleist, E., Wildt, J., Mentel, T. F., Lutz, A., Hallquist, M.,  
695 Worsnop, D., and Thornton, J. A.: A novel method for online analysis of gas and particle composition: description  
696 and evaluation of a Filter Inlet for Gases and AEROSols (FIGAERO), *Atmospheric Measurement Techniques*, 7,  
697 983-1001, 10.5194/amt-7-983-2014, 2014.
- 698 Lopez-Hilfiker, F. D., Mohr, C., D'Ambro, E. L., Lutz, A., Riedel, T. P., Gaston, C. J., Iyer, S., Zhang, Z., Gold,  
699 A., Surratt, J. D., Lee, B. H., Kurten, T., Hu, W. W., Jimenez, J., Hallquist, M., and Thornton, J. A.: Molecular  
700 Composition and Volatility of Organic Aerosol in the Southeastern U.S.: Implications for IEPOX Derived SOA,  
701 *Environ Sci Technol*, 50, 2200-2209, 10.1021/acs.est.5b04769, 2016.
- 702 Mohr, C., Thornton, J. A., Heitto, A., Lopez-Hilfiker, F. D., Lutz, A., Riipinen, I., Hong, J., Donahue, N. M.,  
703 Hallquist, M., Petaja, T., Kulmala, M., and Yli-Juuti, T.: Molecular identification of organic vapors driving  
704 atmospheric nanoparticle growth, *Nat Commun*, 10, 4442, 10.1038/s41467-019-12473-2, 2019.
- 705 Noziere, B., Kalberer, M., Claeys, M., Allan, J., D'Anna, B., Decesari, S., Finessi, E., Glasius, M., Grgic, I.,  
706 Hamilton, J. F., Hoffmann, T., Iinuma, Y., Jaoui, M., Kahnt, A., Kampf, C. J., Kourtchev, I., Maenhaut, W.,  
707 Marsden, N., Saarikoski, S., Schnelle-Kreis, J., Surratt, J. D., Szidat, S., Szmigielski, R., and Wisthaler, A.: The  
708 molecular identification of organic compounds in the atmosphere: state of the art and challenges, *Chem Rev*, 115,  
709 3919-3983, 10.1021/cr5003485, 2015.
- 710 Riipinen, I., Yli-Juuti, T., Pierce, J. R., Petäjä, T., Worsnop, D. R., Kulmala, M., and Donahue, N. M.: The  
711 contribution of organics to atmospheric nanoparticle growth, *Nature Geoscience*, 5, 453-458, 10.1038/ngeo1499,  
712 2012.
- 713 Schauer, J. J., Kleeman, M. J., Cass, G. R., and Simoneit, B. R. T.: Measurement of Emissions from Air Pollution  
714 Sources. 4. C1-C27 Organic Compounds from Cooking with Seed Oils, *Environmental Science & Technology*,  
715 36, 567-575, 10.1021/es002053m, 2002.
- 716 Siegel, K., Zieger, P., Salter, M., Riipinen, I., Ekman, A. M. L., and Mohr, C.: Chemical composition of  
717 summertime High Arctic aerosols using chemical ionization mass spectrometry, May 01, 20202020.
- 718 Siegel, K., Karlsson, L., Zieger, P., Baccarini, A., Schmale, J., Lawler, M., Salter, M., Leck, C., Ekman, A. M. L.,  
719 Riipinen, I., and Mohr, C.: Insights into the molecular composition of semi-volatile aerosols in the summertime  
720 central Arctic Ocean using FIGAERO-CIMS, *Environmental Science: Atmospheres*, 10.1039/d0ea00023j, 2021.
- 721 Tao, J., Zhang, L., Cao, J., and Zhang, R.: A review of current knowledge concerning PM<sub>2.5</sub>  
722 chemical composition, aerosol optical properties and their relationships across China, *Atmospheric Chemistry and*  
723 *Physics*, 17, 9485-9518, 10.5194/acp-17-9485-2017, 2017.
- 724 Thornton, J. A., Mohr, C., Schobesberger, S., D'Ambro, E. L., Lee, B. H., and Lopez-Hilfiker, F. D.: Evaluating  
725 Organic Aerosol Sources and Evolution with a Combined Molecular Composition and Volatility Framework Using



726 the Filter Inlet for Gases and Aerosols (FIGAERO), *Accounts of Chemical Research*, 53, 1415-1426,  
727 10.1021/acs.accounts.0c00259, 2020.

728 Turpin, B. J. and Lim, H.-J.: Species Contributions to PM<sub>2.5</sub> Mass Concentrations: Revisiting Common  
729 Assumptions for Estimating Organic Mass, *Aerosol Science and Technology*, 35, 602-610,  
730 10.1080/02786820119445, 2001.

731 Turpin, B. J., Saxena, P., and Andrews, E.: Measuring and simulating particulate organics in the atmosphere:  
732 problems and prospects, *Atmospheric Environment*, 34, 2983-3013, [https://doi.org/10.1016/S1352-](https://doi.org/10.1016/S1352-2310(99)00501-4)  
733 [2310\(99\)00501-4](https://doi.org/10.1016/S1352-2310(99)00501-4), 2000.

734 Wang, J. M., Jeong, C.-H., Hilker, N., Shairsingh, K. K., Healy, R. M., Sofowote, U., Deboz, J., Su, Y.,  
735 McGaughey, M., Doerksen, G., Munoz, T., White, L., Herod, D., and Evans, G. J.: Near-Road Air Pollutant  
736 Measurements: Accounting for Inter-Site Variability Using Emission Factors, *Environmental Science &*  
737 *Technology*, 52, 9495-9504, 10.1021/acs.est.8b01914, 2018.

738 Watson, J. G. and Chow, J. C.: Comparison and evaluation of in situ and filter carbon measurements at the Fresno  
739 Supersite, *Journal of Geophysical Research: Atmospheres*, 107, ICC 3-1-ICC 3-15, 10.1029/2001jd000573, 2002.

740 Yao, L., Garmash, O., Bianchi, F., Zheng, J., Yan, C., Kontkanen, J., Junninen, H., Mazon, S. B., Ehn, M.,  
741 Paasonen, P., Sipila, M., Wang, M. Y., Wang, X. K., Xiao, S., Chen, H. F., Lu, Y. Q., Zhang, B. W., Wang, D. F.,  
742 Fu, Q. Y., Geng, F. H., Li, L., Wang, H. L., Qiao, L. P., Yang, X., Chen, J. M., Kerminen, V. M., Petaja, T.,  
743 Worsnop, D. R., Kulmala, M., and Wang, L.: Atmospheric new particle formation from sulfuric acid and amines  
744 in a Chinese megacity, *Science*, 361, 278+, 10.1126/science.aao4839, 2018.

745 Yao, L., Fan, X., Yan, C., Kurten, T., Daellenbach, K. R., Li, C., Wang, Y., Guo, Y., Dada, L., Rissanen, M. P.,  
746 Cai, J., Tham, Y. J., Zha, Q., Zhang, S., Du, W., Yu, M., Zheng, F., Zhou, Y., Kontkanen, J., Chan, T., Shen, J.,  
747 Kujansuu, J. T., Kangasluoma, J., Jiang, J., Wang, L., Worsnop, D. R., Petaja, T., Kerminen, V. M., Liu, Y., Chu,  
748 B., He, H., Kulmala, M., and Bianchi, F.: Unprecedented Ambient Sulfur Trioxide (SO<sub>3</sub>) Detection: Possible  
749 Formation Mechanism and Atmospheric Implications, *Environ Sci Technol Lett*, 7, 809-818,  
750 10.1021/acs.estlett.0c00615, 2020.

751 Ye, C., Yuan, B., Lin, Y., Wang, Z., Hu, W., Li, T., Chen, W., Wu, C., Wang, C., Huang, S., Qi, J., Wang, B.,  
752 Wang, C., Song, W., Wang, X., Zheng, E., Krechmer, J. E., Ye, P., Zhang, Z., Wang, X., Worsnop, D. R., and  
753 Shao, M.: Chemical characterization of oxygenated organic compounds in the gas phase and particle phase using  
754 iodide CIMS with FIGAERO in urban air, *Atmos. Chem. Phys.*, 21, 8455-8478, 10.5194/acp-21-8455-2021, 2021.

755 Ylisirniö, A., Barreira, L. M. F., Pullinen, I., Buchholz, A., Jayne, J., Krechmer, J. E., Worsnop, D. R., Virtanen,  
756 A., and Schobesberger, S.: On the calibration of FIGAERO-ToF-CIMS: importance and impact of calibrant  
757 delivery for the particle-phase calibration, *Atmos. Meas. Tech.*, 14, 355-367, 10.5194/amt-14-355-2021, 2021.

758 Zheng, Y., Chen, Q., Cheng, X., Mohr, C., Cai, J., Huang, W., Shrivastava, M., Ye, P., Fu, P., Shi, X., Ge, Y.,  
759 Liao, K., Miao, R., Qiu, X., Koenig, T. K., and Chen, S.: Precursors and Pathways Leading to Enhanced Secondary  
760 Organic Aerosol Formation during Severe Haze Episodes, *Environmental Science & Technology*, 55, 15680-  
761 15693, 10.1021/acs.est.1c04255, 2021.

762